PHASE EQUILIBRIUM STUDIES ON *N*-OXIDATION SYSTEMS TO DETERMINE HOMOGENEOUS MIXTURE CONDITIONS

A Dissertation

by

SUNDER JANARDANAN

Submitted to the Office of Graduate and Professional Studies of
Texas A&M University
in partial fulfillment of the requirements for the degree of

DOCTOR OF PHILOSOPHY

Chair of Committee,	James Holste
Committee Members,	Hae-Kwon Jeong
	Benjamin Wilhite
	Debjyoti Banerjee
Head of Department,	M. Nazmul Karim

December 2018

Major Subject: Chemical Engineering

ABSTRACT

The *N*-oxidation of alkylpyridines is used in the pharmaceutical industries to synthesize alkylpyridine *N*-oxides that are involved in the production of analgesic and anti-inflammatory drugs. The synthesis process involves continuous addition of aqueous hydrogen peroxide (35% w/w) solution to a mixture of alkylpyridine and phosphotungstic acid catalyst. The oxidation is accompanied by undesired decomposition of hydrogen peroxide, which produces large amounts of oxygen and water vapor. This reaction introduces a series of hazards during the operation including the potential to over pressurize an improperly vented reactor and generation of an oxygen-rich atmosphere in an alkyl pyridine flammable environment. The decomposition is accelerated during the *N*-oxidation of higher order alkylpyridines (lutidines, collidines) due to mass transfer limitations caused by the separation of the liquid into organic and aqueous phase. Also, the presence of phosphotungstic acid (catalyst) in the aqueous phase further intensifies the peroxide decomposition reducing the safety and efficiency of the process. It is thus essential to identify homogeneous reaction conditions and operate the reactor in a regime where phase separation is prevented.

The immiscibility between the alkylpyridine and water is primarily responsible for the liquid phase heterogeneity during the *N*-oxidation. The current work addresses this research gap by investigating the influence of the alkylpyridine *N*-oxide on the phase separation since the *N*-oxide is known for its increased reactivity. Experimental and theoretical studies were conducted on 2,6-lutidine/2,6-lutidine-*N*-oxide/water mixtures at different temperatures. The phase equilibrium experiments were conducted at 110 ^{o}C in lab-scale calorimeters wherein the ternary mixtures were analyzed with the help of *in-situ* FTIR spectroscopy. It was found that the extent of heterogeneity between 2,6-lutidine and water is

reduced dramatically by the presence of 2,6-lutidine-*N*-oxide as indicated by the phase diagram.

In order to support the experimental work, the UNIQUAC thermodynamic model was used to estimate the biphasic compositions and predict the LLE curve for the ternary mixture. The energy parameters used in the equations, which describe the intermolecular interactions were calculated based on molecular dynamics simulations. Apart from this, the molecular parameters for *N*-oxide were obtained by following a quantum mechanical approach, which utilized a surface building algorithm for constructing the molecular surface. The results predicted by the model provide a satisfactory representation of the experimental data at T = 110 ^{o}C. In addition to this, the influence of temperature on the phase behavior was studied by generating phase equilibrium data at T = 100 and 125 ^{o}C.

The findings from this research study can be used to implement the inherent safety concept – "Hybridization" to the *N*-oxidation system wherein the concentration of product *N*-oxide can be controlled to maintain a less hazardous environment.

DEDICATION

To my parents who have supported me throughout my journey and provided constant motivation; To all my friends and colleagues

ACKNOWLEDGEMENTS

I cannot express enough thanks to my advisor, Dr. M. Sam Mannan for giving me this opportunity to work with the Mary Kay O' Connor Process Safety Center. I am deeply grateful for his constant support and guidance throughout the course of this research. I also thank him for inspiring me and making me adept at applying the concepts of process safety towards solving real world problems.

I am deeply grateful to Dr. Maria Papadaki (University of Patras, Greece) and Dr. Simon Waldram (MKOPSC) for providing me valuable advice during the course of my research work. I would like to thank Dr. Lisa Perez (Laboratory for Molecular Simulation, Texas A&M University) whose counsel and expertise enhanced my technical skills.

I would like to thank Dr. James Holste, Dr. Benjamin Wilhite and Dr. Debjyoti Banerjee for serving as my committee members and for their assistance during the doctoral program.

Thanks also go to my friends and colleagues and the department faculty and staff for making my time at Texas A&M University a great experience. Finally, thanks to my mother and father for their encouragement and love.

CONTRIBUTORS AND FUNDING SOURCES

Contributors

This work was supported by a dissertation committee consisting of Professor James Holste, Professor Hae-Kwon Jeong and Professor Benjamin Wilhite of the Department of Chemical Engineering and Professor Debjyoti Banerjee of the Department of Mechanical Engineering.

All work for the dissertation was completed by the student, under the advisement of Professor Maria Papadaki (University of Patras, Greece), Dr. Simon Waldram (MKOPSC) and Dr. Lisa Perez (Laboratory for Molecular Simulation, Texas A&M University).

Funding Sources

This research was sponsored by the Mary Kay O' Connor Process Safety Center at Texas A&M University.

TABLE OF CONTENTS

LIST OF FIGURES

Page

LIST OF TABLES

1. INTRODUCTION

Reactivity of a chemical substance is like a 'double-edged sword'. A chemically reactive material is valuable to the process industry since it can be utilized to synthesize a variety of products (Wei, Rogers *et al.* 2004). On the other hand, when plants experience process upsets, (*e.g.,* loss of temperature control, no or insufficient mixing, presence of incompatible materials) these chemicals pose a greater hazard due to their increased reactivity. The resulting incident can be catastrophic leading to an enormous loss to the industry and environment. According to a CSB report, 167 chemical incidents have been triggered by uncontrolled chemical reactivity between 1980 and 2001 in USA (United States Chemical Safety and Hazard Investigation Board 2002). The report identified inadequate hazard identification and lack of process knowledge as the major causes behind these incidents. Since 2001, many other incidents have occurred due to chemically reactive substances underscoring the need for adequate investigation of process hazards and generation of process-related data.

The reactions employed in the pharmaceutical, fine chemical and agrochemical industries are excellent examples of chemical systems, with limited information on chemistry, thermochemistry and thermodynamic properties. In addition to this, the improper understanding of kinetics due to complex reaction systems and non-linear dynamics leads to empirically designed reactors for many of these processes (Pineda-Solano, Saenz-Noval *et al.* 2012). Generally, batch and semi-batch reactors are used to conduct the reactions to accommodate miscellaneous reaction kinetics as well as downstream operations for product separation. Since, these reactors are susceptible to human error, situations leading to deviations from normal

operations occur frequently. Also, large amounts of by-products are generated in the reaction vessels, which can be released into the environment leading to severe pollution. Hence, it is important to enhance the technical know-how of these systems to prevent the occurrence of process safety incidents. Also, this knowledge will aid the implementation of inherently safer alternatives that can lower or eliminate the hazards thereby ensuring safe conditions in the system in the event of abnormal situations.

The *N*-oxidation of alkylpyridine is a reaction employed in the pharmaceutical industry for synthesizing specialty chemicals. The hazards associated with the process arise mainly due to the condition dependent decomposition of hydrogen peroxide, which is used as an oxidant in the reaction. The decomposition reduces the efficiency and hampers the overall safety of the process. The current research aims at evaluating the thermodynamic properties of the reaction mixture at different conditions through experimental and theoretical techniques since they have a direct bearing on the decomposition process. The study can be used to develop inherently safer reactive processes for the *N*-oxidation system, which will result in the design of intensified reactors. Moreover, the alternatives suggested in this work would be applicable to other batch systems with similar characteristics.

1.1 The *N*-oxidation of Alkylpyridines

In the *N*-oxidation reaction, the nitrogen in the pyridine ring structure is oxidized to obtain alkylpyridine *N*-oxide. The oxidizing agent used in the *N*-oxidation reaction is hydrogen peroxide while phosphotungstic acid acts as the catalyst (see reaction scheme (1)).

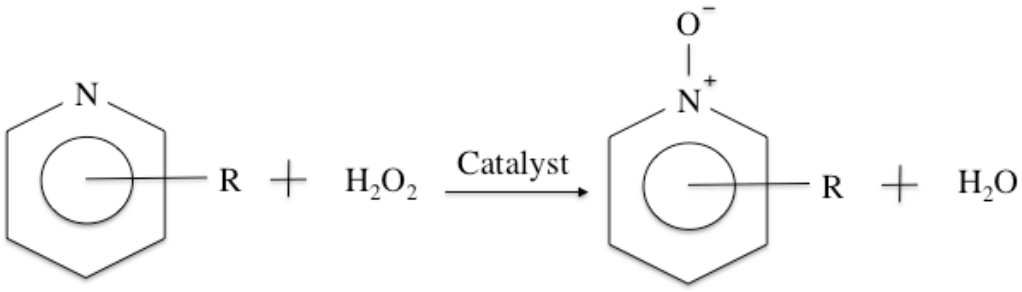

(1)

Open semi-batch reactors are employed in the industry to perform the reaction wherein an aqueous hydrogen peroxide solution (30 – 50%) is added gradually to a system of alkylpyridine and catalyst to avoid excess heat generation. During the process, the reactor temperature is maintained constant and is not allowed to exceed the boiling point of the mixture (90 – 95 °C) (Palomo-Coll 1992; Sempere, Nomen *et al.* 1998). The phosphotungstic acid catalyst promotes the decomposition of hydrogen peroxide along with the *N*-oxidation reaction. Owing to this, excessive amount of hydrogen peroxide is added to the system to achieve the desired conversion. As a result, the reaction mixture has to be neutralized at the end before initiating the separation process. Apart from this, the reactor is connected to an overhead condenser to collect the escaping vapors.

1.1.1. Alkylpyridines

Alkylpyridines are heterocyclic compounds that contain a six membered ring with one nitrogen atom. The ring has alkyl substituents, which increases the basicity of the structure. The alkyl pyridines are classified based on the number of alkyl groups attached to the parent pyridine ring. Monosubstituted rings are known as methyl pyridines (picolines) while di- and trisubstituted

rings are termed lutidines and collidines respectively. The alkylpyridines commonly used in the industry have been shown in Figure 1.

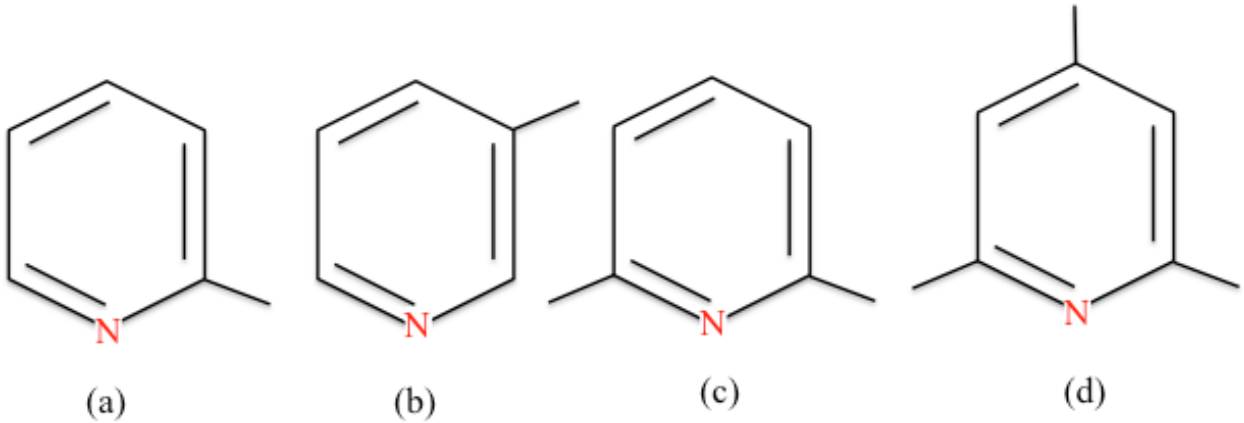

Figure 1. Industrially important alkylpyridines. a) 2-methylpyridine, b) 3-methylpyridine, c) 2,6-dimethylpyridine, d) 2,4,6-trimethylpyridine (2,6-dimethylpyridine was the focus of this work)

Table 1. Physical properties of alkylpyridines (Adapted from (Scriven and Murugan 2000; Shimizu, Watanabe *et al.* 2000))

Chemical	Molecular weight (g/mole)	Melting point (^{o}C)	Boiling point (^{o}C)	Flash point (^{o}C)
2-methylpyridine	93.1	-41.7	129.4	27
3-methylpyridine	93.1	-18.2	144.1	38
2,6-dimethylpyridine	107.2	-6.1	144.5	37
2,4,6-trimethylpyridine	121.2	-43.0	171.5	55

In general, picolines are completely miscible in water while lutidines and collidines exhibit liquid based phase separation when mixed with water at certain conditions. Table 1 displays the physical properties of some alkylpyridines. It can be deduced from the table that these chemicals are flammable with low flash points. Alkylpyridines are widely used in the pharmaceutical and agrochemical industries as chemical intermediates and precursor molecules. For example, a) 2-

methylpyridine is a precursor in the manufacture of 2-vinylchloride, b) 3-methylpyridine is used in the manufacture of an insecticide – chlorpyrifos. Apart from this, they are used as solvents and reagents (Shimizu, Watanabe *et al.* 1993; Scriven and Murugan 2000).

1.1.2. Alkylpyridine N-oxides

Alkylpyridine *N*-oxides are the products of the oxidation of alkylpyridines. Figure 2 shows the structure of 2,6-dimethylpyridine *N*-oxide.

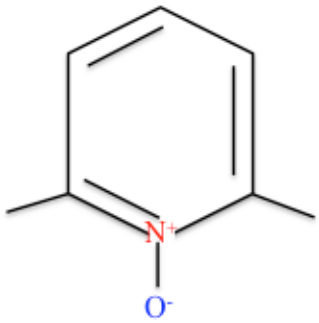

Figure 2. Structure of 2,6-dimethylpyridine *N*-oxide

The *N*-oxide molecule is planar and has higher reactivity than alkylpyridines owing to the presence of both electrophilic and nucleophilic centers. Similar to alkylpyridines, they are used in the pharmaceutical and agrochemical industries as intermediates. They find special applications in the synthesis of analgesics, anti-inflammatory and anti-ulcer drugs. For example, 2,3,5-trimethylpyridine *N*-oxide is used to make omeprazole (an antiulcer drug) (Shimizu, Watanabe *et al.* 1993).

1.1.3. Hydrogen Peroxide

Hydrogen peroxide (H_2O_2) is a clear and colorless liquid. It is an extremely selective oxidizing agent, which reacts with organic and inorganic substances. Additionally, the oxidation reaction with hydrogen peroxide produces water as a byproduct and hence the overall process is environmentally friendly. It is widely used in chemical manufacture, the paper and pulp industry, wastewater treatment, metal finishing, hydrometallurgy and semiconductor wafer cleaning (Jones 1999; Campos-Martin, Blanco-Brieva *et al.* 2006). The physical properties of hydrogen peroxide are included in Table 2.

Table 2. Physical properties of hydrogen peroxide (Adapted from (Jones 1999))

Property	**Value**
Boiling point (^oC)	150.20
Heat of vaporization at 25 ^oC (J/g/K)	1519.00
Specific heat at 25 ^oC (J/g/K)	2.63
Relative density (g/ml)	1.44

Generally, hydrogen peroxide is available as aqueous solutions (≤ 70 wt. %), owing to its miscibility in water. Table 3 shows the properties of hydrogen peroxide solutions.

Table 3. Properties of aqueous hydrogen peroxide solutions
(Adapted from (Jones 1999) and (Yaws 2012))

Property	**30 wt. %**	**50 wt. %**	**60 wt. %**	**70 wt. %**
Density (g/ml)	1.112	1.197	1.242	1.290
Boiling point at 1 atm (^oC)	106	114	119	125
Active O_2 content, %	14.1	23.5	28.2	32.8

Similar to other peroxides, hydrogen peroxide decomposes to oxygen and water vapor at room temperatures due to the unstable peroxy group (−O−O−).

$$H_2O_2 \rightarrow \tfrac{1}{2} O_2 + H_2O \quad (2)$$

This process is exothermic and produces about 98.3 kJ of heat per mole of hydrogen peroxide reacted. It also produces an oxygen-rich flammable environment, which may ignite and cause an explosion in presence of organics. Temperature has a direct effect on the rate of decomposition. The decomposition rate increases by 2.3 times with every 10 ^{o}C rise in temperature. Also, the decomposition is affected by the pH of the reaction system (Jones 1999). Another factor, which influences the decomposition, is the presence of impurities. Alkalis, strong acids (nitric acid) and dissolved salts like iron, chromium and nickel catalyze the reaction homogeneously and increase the decomposition rate. Similarly, insoluble agents like silver, platinum, gold accelerate the reaction (Conner 1993). Incidents involving hydrogen peroxide are common in the industry. Entry of 35% hydrogen peroxide solution (due to suction) from the glove box floor to a pickup vessel containing high concentrations of iron, nickel and copper led to an explosion at Rocky flats, Colorado. The vessel contained radioactive plutonium and the explosion released the radioactive material (Conner 1993). Similarly, a hydrogen peroxide tank car exploded on an expressway in Tokyo due to contamination by copper chloride, which was stored in the tank earlier (Kumasaki 2006). Most of these incidents were a direct result of the decomposition of hydrogen peroxide and the consequent vapor generation (Greene, Baker *et al.* 2005). The above incidents highlight the importance of reducing the accumulation of hydrogen peroxide in any reaction system. Hence, reactions involving hydrogen peroxide are generally carried out in semi-

batch mode wherein hydrogen peroxide is gradually added to the reaction mixture. In a semi-batch operation, the addition of the hydrogen peroxide can be ceased if a reaction runaway occurs (due to cooling failure or excessive accumulation) (Jones 1999). Similarly, it is a common practice to add stabilizers to aqueous hydrogen peroxide solutions to lower the decomposition rate during storage.

1.1.4. Phosphotungstic acid

Phosphotungstic acid ($H_3PW_{12}O_{40}.nH_2O$) is a white solid, which is used as a catalyst in the *N*-oxidation process. It is a type of heteropolyacid and belongs to the Keggin series. It has a characteristic structure consisting of a central PO_4 tetrahedron and 12 edge-sharing WO_6 octahedrons surrounding. Phosphotungstic acid can form hydrogen bonds with water molecules and hence it is soluble in water. PTA completely dissociates in water releasing heteropolyanions $(PW_{12}O_{40})^{-3}$ (see Figure 3). On the contrary, the solubility of PTA is low in organic solutions owing to its inability to interact with organic molecules (Kozhevnikov, Sinnema *et al.* 1995).

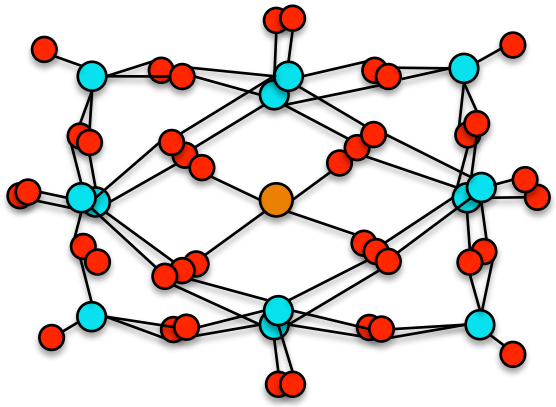

Figure 3. Structure of phosphotungstate anion (Phosphorus atom is denoted by orange while tungsten and oxygen atoms are represented by blue and red respectively) (Kozhevnikov 2007).

Phosphotungstic acid has been used widely in industrial processes like esterification's, polymerizations, hydrations due to its high selectivity and activity (Brønsted acidity) (Kozhevnikov 1987). Also, the catalyst is reusable and thermally stable up to temperatures of 465 ^{o}C (Kozhevnikov 2007). Apart from this, catalyst is non-toxic, non-corrosive and non-volatile (Misono, Ono *et al.* 2000).

1.2. Hazards associated with the *N*-oxidation process

As discussed above, the hydrogen peroxide has a strong tendency to decompose. Hence, the *N*-oxidation reaction is accompanied by the undesired decomposition of hydrogen peroxide, which reduces the overall yield and selectivity of the process. Apart from this, a runaway of this reaction may lead to a tremendous increase in the temperature in the reactor and generate large amounts of gaseous oxygen and water vapor. This temperature rise might lead to decomposition of the reaction products (*N*-oxides) producing non-condensable gases, which will lead to a further increase in the pressure and temperature in the reactor. The oxygen rich environment poses a major fire and explosion hazard due to the flammable nature of alkyl pyridines. Also, the rapid generation of gas can over pressurize a closed reactor and lead to secondary decompositions hampering the overall safety of the process.

Secondly, higher order alkyl pyridines (*e.g.*, lutidines and collidines) have limited miscibility in water. Therefore, during the synthesis of higher order *N*-oxides, two – phase systems can be formed (*i.e.*, organic and aqueous) wherein the reaction takes place at the interface. Hence, the

mass transfer of the reactants and catalyst to the interface influences the overall reaction rate. The solid catalyst has poor solubility in the organic phase and remains in the aqueous phase accelerating the decomposition of the hydrogen peroxide. This reduces the efficiency and selectivity of the process by reducing the amount of hydrogen peroxide utilized in the oxidation reaction. Hence, it is very important to avoid operating conditions where a heterogeneous mixture is obtained (Saenz-Noval 2011; Pineda-Solano 2014).

2. LITERATURE REVIEW

The *N*-oxidation of alkylpyridines can serve as a model reaction for other complex batch systems utilizing reactive chemicals like peroxides and metal catalysts. Hence, various researchers have studied this system with an objective of increasing the product yield and enhancing the process safety (Sempere, Nomen *et al.* 1998; Papadaki, Emery *et al.* 2002; Papadaki, Stoikou *et al.* 2002; Papadaki and Nawada 2003; Papadaki and Gao 2005; Papadaki, Marqués-Domingo *et al.* 2005; Gao and Papadaki 2006). Most of the work on the *N*-oxidation of alkylpyridines has been concentrated on developing kinetic models for the reaction, which can predict the alkypyridine conversion at various temperatures, pressures and initial compositions. Research has also been focused on identifying inherently safer operating conditions for the process where the peroxide decomposition is minimized. In order to achieve these objectives, the *N*-oxidation reaction was conducted in calorimeters used both as open and closed systems.

The initial studies were realized in open reactors working at atmospheric pressures wherein the system temperature was maintained between 85 and 100 ^{o}C. Sempere, Nomen *et al.* (1998) performed the *N*-oxidation of 2-picoline at three different temperatures (85, 93 and 100 ^{o}C) in a semi-batch system wherein aqueous solutions of hydrogen peroxide were added to the picoline/catalyst mixture over a fixed period of time. Based on the thermal profiles, it was clear that the reaction did not follow the simple power law model. Hence, the authors adopted the Langmuir-Hinshelwood approach, which considers the reaction as a series of fast equilibrium steps wherein the reactants combine with the catalyst sites to generate intermediates that result in

the final products. The model parameters were predicted by reducing the error between the calculated profiles and the experimental results.

Papadaki and Gao (2005) extended this work to other alkyl pyridines (*i.e.*, 3-picoline, 2,6-lutidine, 3,5-lutidine and 2,4,6-collidine) and modified the existing model. They neglected all reaction pathways which were non-catalytic and found that the resultant model could represent the calorimetric data more accurately. Nevertheless, the rate and equilibrium constants included in the model could not be evaluated with sufficient reliability. Also, the model showed partial agreement in describing the *N*-oxidation of high order alkylpyridines (lutidines and collidines) owing to liquid-liquid demixing during the reaction, which increased the kinetic complexity.

While performing the *N*-oxidation reaction in open reactors, a limited temperate range (essentially between 85 and 100 ^{o}C) was employed. The decomposition reaction was vigorous at temperatures below 85 ^{o}C, leaving minute quantities of hydrogen peroxide to react with the alkylpyridine. On the other hand, the *N*-oxidation reaction was more prominent at higher temperatures indicating that the decomposition rate is reduced with an increase in temperature. However, since the boiling point of the reaction mixture is around 100 ^{o}C, the maximum temperature of the reaction had to be maintained below this limiting value.

A similar effect was seen when the quantity of catalyst in the mixture was varied. A higher catalyst concentration favored the *N*-oxidation by suppressing the decomposition reaction. Owing to this, the *N*-oxidation reaction occurred at rapid rates and only limited kinetic data could be collected during the experiments. At lower catalyst concentration, the *N*-oxidation reaction

depended on the availability of hydrogen peroxide in the solution, which was determined by the peroxide addition rate. Since the reaction was dosing controlled, it was difficult to generate sufficient kinetic information under these conditions as well. Hence, the kinetic study of *N*-oxidation of alkypyridines is fundamentally complex.

In addition to this, the peroxide decomposition reaction depends on the alkalinity of the solution. It was found that the rate of catalytic decomposition of hydrogen peroxide was slower in presence of alkylpyridines than in their absence (Papadaki, Stoikou *et al.* 2002). Hence, the peroxide decomposition reaction is condition-sensitive and should be studied along with the *N*-oxidation reaction.

In short, the results indicate that the safety and efficiency of the *N*-oxidation reaction are affected by various factors like temperature, pressure, catalyst concentration and mixing in the system. Therefore, it was suggested that the reaction should be operated in the single-phase regime and higher temperatures (>100 ^{o}C) and pressures should be employed while conducting the reaction.

Based on these findings, Saenz-Noval (2011) addressed the following issues in her work, (i) Effect of higher temperatures and pressures on the *N*-oxidation reaction, (ii) Study of decomposition of alkylpyridines and alkylpyridine *N*-oxides, (iii) Influence of alkylpyridine *N*-oxide on the decomposition of hydrogen peroxide.

In order to operate the *N*-oxidation reaction at elevated temperatures, an isothermal calorimeter was employed which had the ability to withstand high pressures. Using this apparatus, the *N*-

oxidation of 2-picoline and 2,6-lutidine were studied by Saenz-Noval (2011) at process temperatures ranging from 110 ^{o}C to 125 ^{o}C. The experiments indicated that stoichiometric amounts of hydrogen peroxide could convert 98% (or more) of the 2-picoline into *N*-oxide. Nevertheless, the influence of the catalyst on the reaction efficiency could not be ascertained. During the 2,6-lutidine *N*-oxidation, it was observed that the organic/water phase separation led to excessive decomposition of hydrogen peroxide even at increased temperatures. The agitator speeds were varied during the trials in order to enhance the mixing between the chemical species. However, the decomposition rate was rapid and the reactor had to be vented frequently owing to the buildup of oxygen gas.

Secondly, adiabatic experiments were performed on 2-picoline and 2-picoline *N*-oxide to determine their stability and decomposition pathways (Saenz, Vazquez *et al.* 2009; Saenz, Carreto-Vazquez *et al.* 2011). 2-picoline did not decompose in the presence/absence of the catalyst and remained stable up to 350 ^{o}C. On the other hand, the decomposition of 2-picoline *N*-oxide was substantial at temperatures in excess of 200 ^{o}C. Also, the catalyst had a positive impact on the decomposition reaction. Moreover, the decomposition produced non-condensable gases, which could be detrimental to the safety of the *N*-oxidation process.

Similarly, when the decomposition of hydrogen peroxide was investigated, it was observed that the reaction rate decreased with a reduction in the catalyst concentration. In addition to this, the decomposition temperature of the hydrogen peroxide was lowered substantially by the presence of 2-picoline *N*-oxide. Likewise, the 2-picoline *N*-oxide decomposition occurred at lower temperatures in presence of the hydrogen peroxide.

Pineda Solano (2014) extended this work to other members of the alkylpyridine family. 3-picoline was studied to investigate the effect of temperature, catalyst concentration, peroxide addition rate and stirring rate. The experiments suggested that the increase in temperature from 110 ^{o}C to 125 ^{o}C did not reduce the decomposition significantly (Pineda-Solano, Saenz-Noval *et al.* 2012). Hence it was concluded that the rise in temperature could be favorable only up to a certain extent. The amount of catalyst employed during the *N*-oxidation had a similar impact on the decomposition. Apart from this, a 2^4 factorial design of experiments indicated that the catalyst concentration and the peroxide-dosing rate are the major factors influencing the overall conversion of the 3-picoline.

The results obtained from the *N*-oxidation of 3,5-lutidine were almost identical to the first case. On the other hand, the *N*-oxidation of 2,6-lutidine and 2,4,6-collidine were characterized by the formation of two liquid phases, which led to the vigorous decomposition of the hydrogen peroxide.

The thermal stability studies on 3-picoline, 2,6-lutidine, 3,5-lutidine and 2,4,6-collidine revealed that these chemicals were stable up to 400 ^{o}C. The corresponding alkylpyridine *N*-oxides decomposed producing non-condensable gases when exposed to temperatures in excess of 230 ^{o}C (Pineda Solano 2014).

In general, previous research has focused on improving the understanding of this complex reactive system in order to enhance the safety and efficiency of the process. All the findings have

underscored the importance of identifying operating conditions that can maintain homogeneity in the mixture during the reaction, especially during the *N*-oxidation of lutidines and collidines.

To that end, Saenz-Noval (2011) suggested the addition of an external chemical to the mixture for resolving the problem of phase separation. In order to substantiate this claim, the three-component system containing 2,6-lutidine, water and acetic acid was investigated in process simulator software using the Gibbs minimization method. The results show that the two-phase region between 2,6-lutidine and water shrinks in the presence of acetic acid.

3. MOTIVATION AND RESEARCH SCOPE

Elimination or mitigation of reactive hazards can be achieved by implementing the Inherent Safety concepts introduced by Trevor Kletz (Kletz 1978; Kletz 1985). According to Kletz, the four major approaches for making process plants inherently safer include a) Minimization (Reduce quantities of hazardous chemicals), b) Substitution (Replace hazardous chemicals with safer ones), c) Attenuation (Operate at conditions that are less hazardous) and d) Simplification (Reduce system complexities to reduce operator errors). Since its inception these strategies have been applied to the various stages of a plant lifecycle including research and development phase, design phase, operation and maintenance phase and final decommissioning phase. Apart from this, many new modifications, ideas and techniques have been suggested in the last two decades to broaden the scope of this topic.

Edwards (2011) presented a new inherent safety technique based on the work of Chen (2004). This concept was termed as hybridization/transformation and involved the introduction of an external inert chemical into a potentially hazardous reaction system to make it less hazardous while retaining the fundamental chemistry. In his study, Chen (2004) found that introducing water during cyclohexane oxidation increases the vapor pressure of the mixture due to formation of a minimum-boiling azeotrope between cyclohexane and water. This decreases the deflagration hazard of the process by reducing the UFL of cyclohexane in oxygen during the oxidation. Apart from this, the added water does not react with the cyclohexane thereby the reaction chemistry remains unaltered. The overall approach is an example of hybridization, wherein water acts as the inert agent that makes the process inherently safer without interfering with the reaction. In addition to this, the adopted method provides an opportunity to enhance the overall

productivity of the reaction by using pure oxygen (instead of air) for the oxidation, which was previously avoided to prevent flammable conditions. The current research is aimed at identifying a similar prospect for the *N*-oxidation of higher order alkyl pyridines by addressing the problem of liquid-liquid de-mixing during the reaction in an inherently safer manner.

The liquid phase heterogeneity observed during the *N*-oxidation of higher order alkylpyridines could be attributed to the immiscibility between alkylpyridine and water. Andon and Cox (1952) studied the phase diagram for a system of 2,6-lutidine and water over a wide temperature region (30 to 230 °C). They found that adding 3-picoline to a mixture of 2,6-lutidine and water reduces the immiscibility between the two species. Similar results were obtained with acetic acid as shown by Sanez-Noval (2011). This indicates that the addition of a third component to the binary system can bring about homogeneity in the solution. However, if the added component has a tendency to react with the chemicals in the *N*-oxidation system then the selectivity of the process will still be compromised. Also, separation of the byproducts formed due to the undesired reaction will increase the overall cost associated with the process. In this case, it would be worthwhile to study the effect of the product *N*-oxide on the alkylpyridine-water phase separation. The *N*-oxide is expected to have a positive impact on the mixing in the *N*-oxidation system since it more soluble in water as compared to the parent alkylpyridine. Moreover, it was found that the two-phase mixtures obtained at the start of the *N*-oxidation of 2,6-lutidine and 2,4,6-collidine disappeared slowly as the reaction progressed towards the end (Pineda Solano 2014). Currently, phase equilibrium data for mixtures containing alkylpyridine *N*-oxides are not available in the literature. A complete phase diagram of the components involved in the *N*-oxidation system could identify the minimum composition of *N*-oxide that could prevent the formation of two liquid phases during the entire process and enhance safety and productivity.

This result could be used to operate the reaction in the homogeneous regime by adding adequate amounts of *N*-oxide to the initial mixture or by dosing it during the reaction. The strategy would be an example of the hybridization concept discussed in the previous section.

The current work initiates research in this area by developing phase diagrams for the three-component system containing 2,6-lutidine, 2,6-lutidine-*N*-oxide and water at various temperatures. 2,6-lutidine *N*-oxidation represents a case where large amounts of hydrogen peroxide were required to achieve the desired conversions owing to the heterogeneity in the solution. Another factor, which was considered while selecting this system, was the availability of liquid-liquid equilibrium data for 2,6-lutidine/water binary mixtures published by various authors over extended temperature ranges (Andon and Cox 1952; Cox and Herington 1956; Grattoni, Dawe *et al.* 1993; Stephenson 1993). The major objectives of this work can be summarized as follows:

- Inspection of ternary mixtures of 2,6-lutidine, 2,6-lutidine-*N*-oxide and water to identify the homogeneous and heterogeneous compositions. In addition to this, the liquid-liquid ternary diagram was constructed to demarcate the singe and two-phase region.

- To evaluate the use of *in-situ* Fourier Transform Infrared (FTIR) spectroscopy as an analytical tool to successfully differentiate between the homogeneous and heterogeneous solutions of 2,6-lutidine, 2,6-lutidine-*N*-oxide and water.

- To evaluate the applicability of computational chemistry in determining the binary energy parameters for the system at various temperatures.

- To estimate the biphasic compositions and predict the LLE curve for the ternary mixture using UNIQUAC activity coefficient model in combination with computational chemistry. In addition to this, the influence of temperature on the phase behavior was studied by constructing phase diagrams at different temperatures.

In general, the results of this study will enhance the thermodynamic understanding of the three-component system, which will assist future studies in this direction. Also, the present work could be extended to other higher order alkylpyridines to verify if a similar relation exists between the aqueous solutions of alkylpyridine and their corresponding *N*-oxides. This can facilitate the design of improved reactors for the *N*-oxidation process that are inherently safer and cost effective.

4. STUDY OF TERNARY MIXTURES OF 2,6-LUTIDINE/2,6-LUTIDINE-*N*-OXIDE/WATER USING ISOTHERMAL CALORIMETER AND FOURIER TRANSFORM INFRARED TECHNOLOGY[1]

The following section provides details regarding the phase equilibrium experiments conducted on the three component system of 2,6-lutidine, 2,6-lutidine-*N*-oxide and water. The experiments were performed in the Mettler-Toledo RC1*e* isothermal calorimeter at Texas A&M University at College Station. The calorimeter was used to maintain the liquid solutions at the desired temperature with continuous mixing to ensure that equilibrium is attained in reasonable time. The RC1*e* was equipped with an FTIR probe, which was used to collect the infrared spectra of the liquid mixtures contained in the vessel. This data was used to distinguish between single phase and biphasic mixtures and identify the compositions where phase separation occurred in the ternary solutions. The hardware configuration of the RC1*e* has been described in subsection 4.1 along with its functional capabilities. Also, this section discusses the operational details of the FTIR spectrometer employed in the current study. Subsection 4.2 incorporates details regarding the experimental procedure followed in this research to perform the phase equilibrium trials. The results obtained from the experiments and the analysis of the FTIR spectral data have been presented in subsection 4.3. The conclusions from this study have been summarized in subsection 4.4.

[1] Part of this section is reprinted with permission from 'Janardanan, S., M. I. Papadaki, S. P. Waldram *et al.* (2017). "Toward an inherently safer alternative for operating N-oxidation of alkylpyridines: Effect of N-oxide on lutidine – water phase separation." Thermochimica acta **656**(Supplement C): 38-46', Copyright [2017] by Elsevier.

4.1. Equipment Description

4.1.1. Mettler-Toledo RC1e Isothermal Calorimeter

The Mettler-Toledo's RC1*e* MP10 is a 1.2 L fully automated small-scale glass jacketed reactor used to study reactive chemical systems. The calorimeter is equipped with a platinum resistance thermometer, pressure gauge and rupture disc (set at 12 barg) for measuring the temperature and pressure inside the vessel and ensuring safety during normal operations. Apart from this, an anchor stirrer (diameter 10.5 cm, height 6.7 cm and length 44 cm) made of Hastealloy provides constant agitation to the reactor contents.

A thermostat regulates the temperature of the reactor by circulating silicone oil through the jacket. The thermostat contains a hot oil reservoir and cold oil reservoir. In order to attain the required temperature, requisite amounts of hot oil and cold oil are mixed before passing the oil around the jacket. An electrical heater is used to heat the hot oil reservoir while the cold oil reservoir is in contact with a cooling coil that passes through a chiller unit. Also, high oil circulation velocities are maintained in the jacket to achieve constant temperatures. A second platinum resistance thermometer has been provided in the jacket for temperature measurement.
In addition to this, a separate external cooling/heating Julabo bath was used to heat the reactor lid to minimize heat losses to the surrounding and maintain better temperature control. The maximum operating temperature of the RC1*e* reactor is 162 °C.

A pressure controller regulates the reactor pressure and the maximum operating pressure is 10 barg. During the experiments, the pressure controller was inactive and the total pressure of the

system was equal to the sum of the air pressure and vapor pressure of the mixture. Apart from this, a ProMinent® solenoid-metering pump is included with the or the purpose of adding materials to the reactor,

A Universal Control Box (UCB) connects the equipment to the personal computer (PC) which is used to operate the three modules of the RC1*e* *i.e.*, electronic control and monitoring system, thermostat and measuring system. The temperature and pressure of the reactor, temperature of the circulating oil and stirring speed are recorded every two seconds by a microprocessor which relays the data to the PC. Furthermore, the calorimeter incorporates the *iControl* software for data processing. Figure 4 shows the schematic for the RC1*e* employed in the current work (Mettler-Toledo 2012).

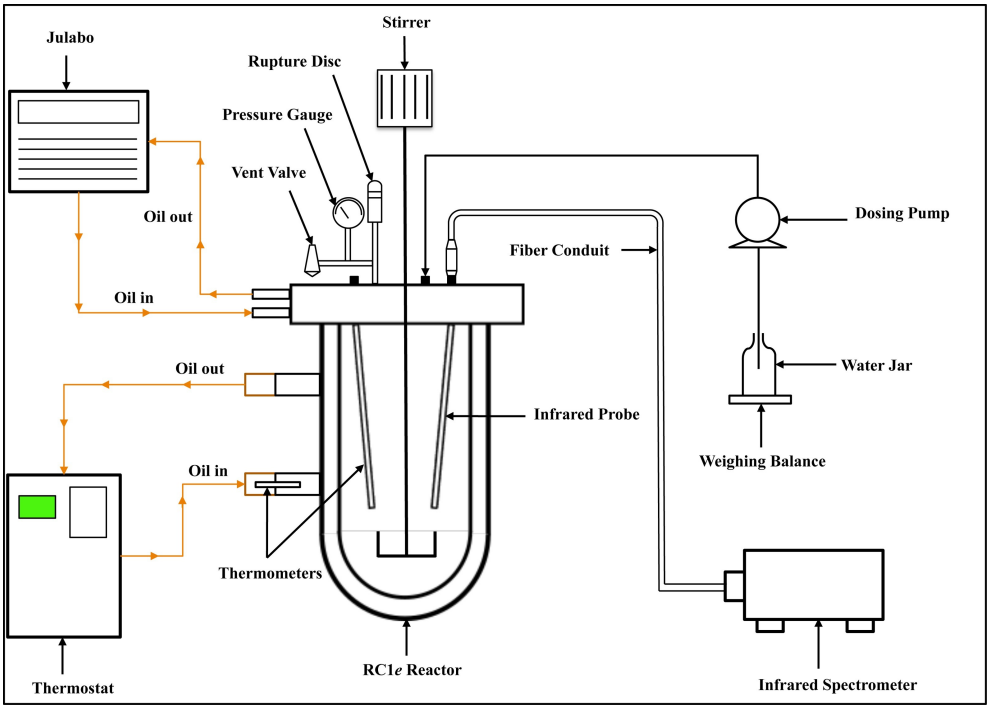

Figure 4. Schematic representation of the RC1*e* (Reprinted with permission from (Janardanan, Papadaki *et al.* 2017))

4.1.2. ReactIR 15™

ReactIR 15™ is an infrared spectrometer which has the capability to identify chemical species in any liquid mixture. Based on the Fourier Transform Infrared (FTIR) Technology, the instrument can analyze chemical systems non-intrusively. The equipment consists of a sampling probe with a diamond-composite sensor at the tip (DiComp™) that can be inserted into the RC1*e* reactor. The infrared light from the ReactIR 15™ source is transferred to the probe tip through a DS Fiber Conduit containing silver halide fibers. The transmitted signal travels through the fibers and is received by a liquid-nitrogen cooled Mercury Cadmium Telluride (MCT) detector. Silica gel is used to maintain dry conditions inside the instrument and prevent any interference from water vapor. The instrument transmits the information to a PC and the iC IR 4.2 Mettler Toledo software is used to analyze the collected infrared data (Mettler-Toledo 2012).

4.2. Experimental Procedure

The experiments were conducted at 110 °C in the RC1*e* calorimeter. Ternary compositions of 2,6-lutidine (lutidine), 2,6-lutidine-*N*-oxide (*N*-oxide) and water were obtained by diluting binary and ternary solutions with water. Information regarding the purity of the chemicals used in the study is included in Table 4.

Table 4. List of chemicals used in this research **(**Reprinted with permission from (Janardanan, Papadaki *et al.* 2017))

Chemical Name	CAS number	Source	Mass Fraction Purity[a]
2,6-lutidine (lutidine)	108-48-5	Sigma-Aldrich	0.98
2,6-lutidine-*N*-oxide (*N*-oxide)	1073-22-0	Chem-Impex International Inc.	0.98
Water	7732-18-5	Utilities & Energy Services – Texas A&M University	0.9999

[a] Chemical were used without purification

The following procedure was employed during the dilution experiments. A mixture of known composition was prepared and loaded into the RC1*e* reactor at ambient temperature. The ATR-FTIR probe was inserted into the liquid medium and the reactor was completely sealed to maintain an airtight arrangement. Before introducing the probe inside the reactor, the tip was washed with acetone and dried to prevent contamination from previous trials. After sealing the reactor, the stirrer was activated and maintained at 200 rpm to provide constant agitation to the liquid contents. The reactor was heated to 110 °C by raising the temperature setpoint of the oil in the jacket. Once the required temperature was attained, the system was left to stabilize for 45 − 90 min before initiating the dilution process. The metering pump was used to dose water (at ambient temperature) into the reactor at a fixed rate to alter the concentration of the mixture. The dosing process was periodic and was halted to add equivalent amounts of water in each interval.

After each addition interval, the system was given 20 − 35 min for achieving thermal equilibrium. Once the temperature was steady and within ±0.03 ^{o}C of the desired temperature (110 °C), the system was inspected visually to look for signs of phase separation. Also, the FTIR probe was used to collect infrared spectra of the liquid mixture (5 − 10 scans) with a resolution

of 8 cm^{-1}. For biphasic systems, the stirrer was stopped momentarily after collecting the absorption spectra and the system was allowed to rest for 30 − 45 min before observing the separated phases. The reactor was cooled back to room temperature at the end of the dosing process.

4.3. Results and Discussion

4.3.1. Dilution experiments

Five binary mixtures of lutidine and *N*-oxide (90/10, 85/15, 80/20, 75/25, 60/40 wt.%) were considered for dilution. Initial mixtures were homogeneous, clear and yellow in color. As water was dosed into the system, the solution got progressively darker until it lost its transparency and became cloudy. As mentioned in the previous section, the system was stabilized, inspected and scanned after fixed dosing intervals. Table 5 provides details regarding the mixtures that were analyzed during the process. When the stirrer was stopped to examine the cloudy solutions the mixtures separated into two distinct transparent liquid layers (upper layer had a brown color while the lower layer was faintly yellow) with a well-defined interface at equilibrium. This confirmed that the system had undergone demixing and marked the end of the experiment. The ternary mixtures obtained during the dilution of the 60/40 mixture remained clear during the entire dosing period.

Table 5. Experimental equilibrium mass fractions *w* for the system 2,6-lutidine (1) + 2,6-lutidine-*N*-oxide + water (3) at temperature T = 110 °C and pressure P = 0.1 MPa (first set of dilution experiments) (Reprinted with permission from (Janardanan, Papadaki *et al*. 2017)) [a,b,c]

T/C	$w_1 \times 100$	$w_2 \times 100$	$w_3 \times 100$	
110	90.00	10.00	-	P0
110	83.12	9.49	7.39	P1
110	77.40	8.84	13.76	P2
110	72.42	8.27	19.31	P3
110	68.04	7.77	24.19	P4
110	64.16	7.33	28.51	P5
110	85.00	15.00	-	-
110	78.63	13.98	7.40	-
110	73.21	13.01	13.77	-
110	68.50	12.18	19.33	-
110	64.35	11.44	24.21	-
110	60.68	10.79	28.53	-
110	57.40	10.20	32.39	-
110	80.00	20.00	-	Q0
110	74.15	18.43	7.42	Q1
110	69.03	17.16	13.81	Q2
110	64.57	16.05	19.38	Q3
110	60.65	15.08	24.27	Q4
110	57.18	14.22	28.60	Q5
110	54.09	13.45	32.47	Q6
110	51.31	12.76	35.93	Q7
110	48.80	12.13	39.06	Q8
110	75.00	25.00	-	-
110	47.90	16.12	35.98	-
110	46.06	15.50	38.43	-
110	44.37	14.93	40.70	-
110	42.79	14.40	42.81	-
110	41.32	13.91	44.77	-
110	39.95	13.45	46.60	-
110	60.00	40.00	-	R0
110	55.64	36.97	7.39	R1
110	51.81	34.42	13.76	R2
110	48.48	32.21	19.32	R3
110	45.54	30.26	24.20	R4
110	42.95	28.53	28.52	R5
110	40.63	26.99	32.38	R6
110	38.55	25.61	35.84	R7
110	36.67	24.36	38.97	R8
110	34.97	23.23	41.80	R9
110	33.41	22.20	44.38	R10
110	31.99	21.26	46.75	R11
110	30.69	20.39	48.92	R12
110	29.49	19.59	50.92	-
110	28.38	18.85	52.77	-
110	27.35	18.17	54.49	-
110	26.39	17.53	56.08	-

Table 5. Continued

T/C	$w_1 \times 100$	$w_2 \times 100$	$w_3 \times 100$	
110	25.49	16.94	57.57	-
110	24.43	16.23	59.34	-
110	23.00	15.28	61.72	-
110	21.73	14.44	63.84	-
110	20.59	13.68	65.73	-
110	19.56	13.00	67.44	-
110	17.79	11.82	70.39	-
110	16.31	10.84	72.85	-
110	15.66	10.41	73.93	-

[a] Standard uncertainties *u* are $u(T) = 0.002$ °C, $u(P) = 1$ kPa and $u(w) = 0.001$
[b] Heterogeneous mixtures (cloudy solutions) have been highlighted in grey. These are not actual binodal data points and lie inside the phase separation region
[c] Letter-number designations denote mixtures probed by ATR-FTIR

In order to determine the phase separation compositions with more certainty, a second set of dilution experiments was performed with two ternary mixtures. Results from these trials have been incorporated in Table 6. As we can see, the compositions of the starting mixtures correspond to homogeneous solutions obtained during the dilution of 90/10 and 80/20 lutidine + *N*-oxide mixture (P3 and Q7). During this study, the quantity of water added in each step was reduced to spot the transition between the homogeneous and heterogeneous mixtures more accurately.

Table 6. Experimental equilibrium mass fractions *w* for the system 2,6-lutidine (1) + 2,6-lutidine-*N*-oxide + water (3) at temperature $T = 110$ °C and pressure $P = 0.1$ MPa (second set of dilution experiments)(Reprinted with permission from (Janardanan, Papadaki *et al*. 2017)) [a,b]

T/C	$w_1 \times 100$	$w_2 \times 100$	$w_3 \times 100$
110	72.39	8.07	19.55
110	72.10	8.04	19.86
110	71.82	8.00	20.18
110	71.26	7.94	20.80
110	70.70	7.88	21.42
110	70.16	7.82	22.02

Table 6. Continued

T/C	$w_1 \times 100$	$w_2 \times 100$	$w_3 \times 100$
110	69.62	7.76	22.61
110	69.10	7.70	23.20
110	68.58	7.64	23.78
110	68.07	7.59	24.35
110	67.56	7.53	24.91
110	67.31	7.50	25.18
110	67.07	7.48	25.46
110	51.14	12.85	36.00
110	51.01	12.82	36.17
110	50.88	12.78	36.33
110	50.76	12.75	36.49
110	50.63	12.72	36.65
110	50.50	12.69	36.81
110	50.37	12.66	36.97
110	50.25	12.62	37.13
110	50.12	12.59	37.29
110	50.00	12.56	37.44
110	49.87	12.53	37.60
110	49.75	12.50	37.75
110	49.62	12.47	37.91

[a] Standard uncertainties u are $u(T) = 0.002$ °C, $u(P) = 1$ kPa and $u(w) = 0.001$
[b] Heterogeneous mixtures (cloudy solutions) have been highlighted in grey. These are not actual binodal data points and lie inside the phase separation region

The results obtained from the dilution experiments were represented on a triangular diagram to identify the single and two phase envelopes. Binary mixtures of lutidine and *N*-oxide are represented on the side of the triangle while the ternary solutions have been indicated as points inside the triangle (see Figure 5 and 6). Based on the data, a binodal curve was constructed (shown in Figure 7) to demarcate the homogeneous and heterogeneous regions for the system. If the mixture composition lies in the shaded region then the system will exhibit phase separation and exist as two phases (organic and aqueous) while a single liquid phase will be seen for compositions in the unshaded area. It can be inferred that the *N*-oxide increases the extent of

homogeneity between lutidine and water. Moreover, it is safe to assume that the three-component system will remain homogeneous if the *N*-oxide concentration is maintained above 20% for any combination of lutidine and water at 110 °C. Apart from this, another important observation was made while cooling the mixtures back to room temperature. It was seen that turbid mixtures regained transparency as the temperature of the system was reduced indicating that lesser quantities of *N*-oxide might be required to homogenize the mixtures at lower temperatures.

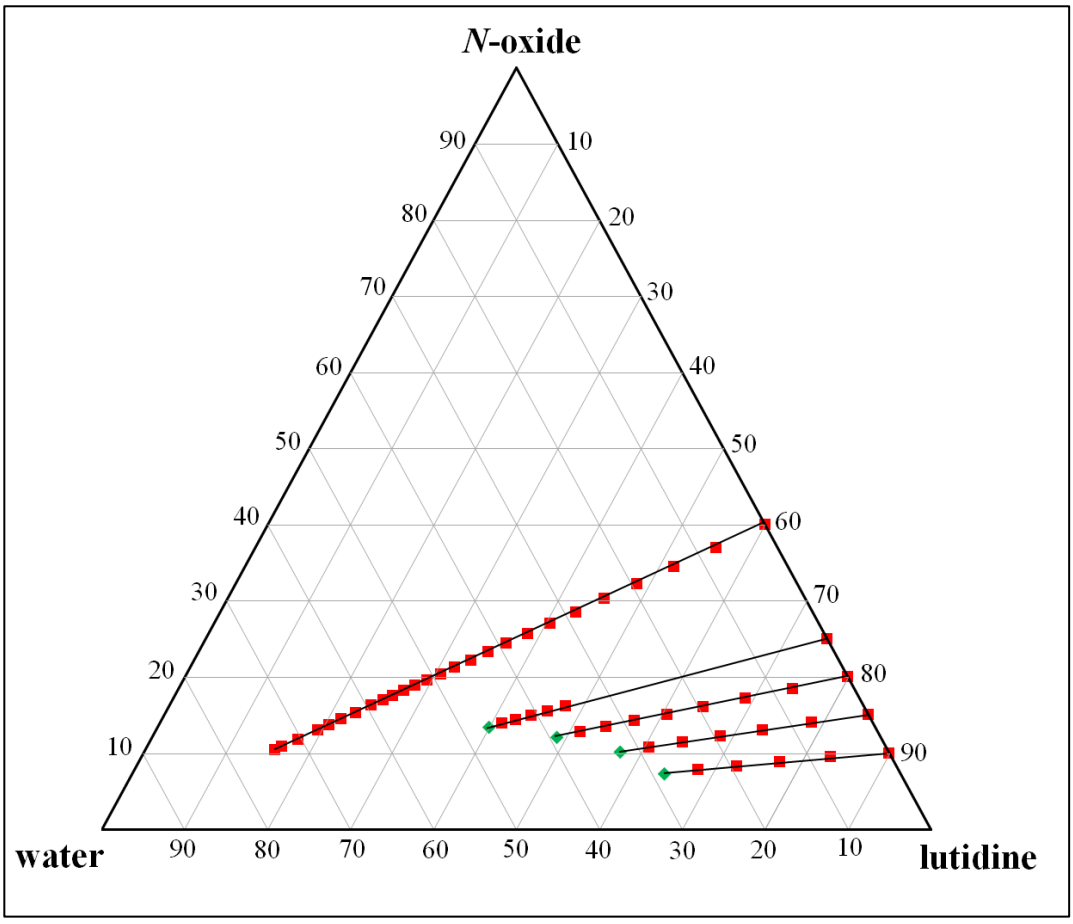

Figure 5. Ternary diagram for the system 2,6-lutidine (lutidine) + 2,6-lutidine-*N*-oxide (*N*-oxide) + water showing ternary mixtures from first set of dilution experiments
Homogenous mixtures are denoted by ■ ,while heterogeneous mixtures are denoted by ◆
(Reprinted with permission from (Janardanan, Papadaki *et al*. 2017))

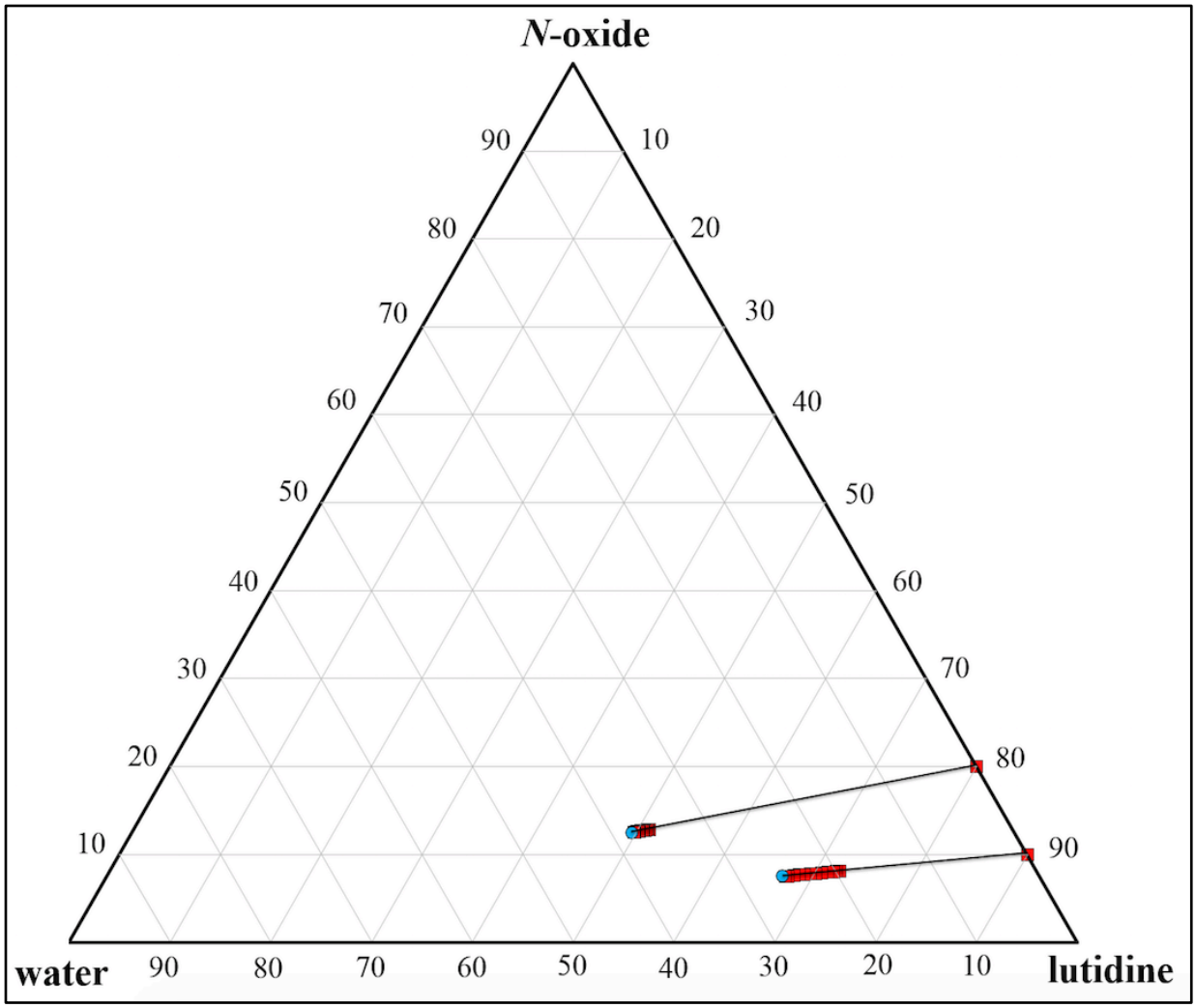

Figure 6. Ternary diagram for the system 2,6-lutidine (lutidine) + 2,6-lutidine-*N*-oxide (*N*-oxide) + water showing ternary mixtures from second set of dilution experiments
Homogenous mixtures are denoted by ■, while heterogeneous mixtures are denoted by ●
(Reprinted with permission from (Janardanan, Papadaki *et al*. 2017))

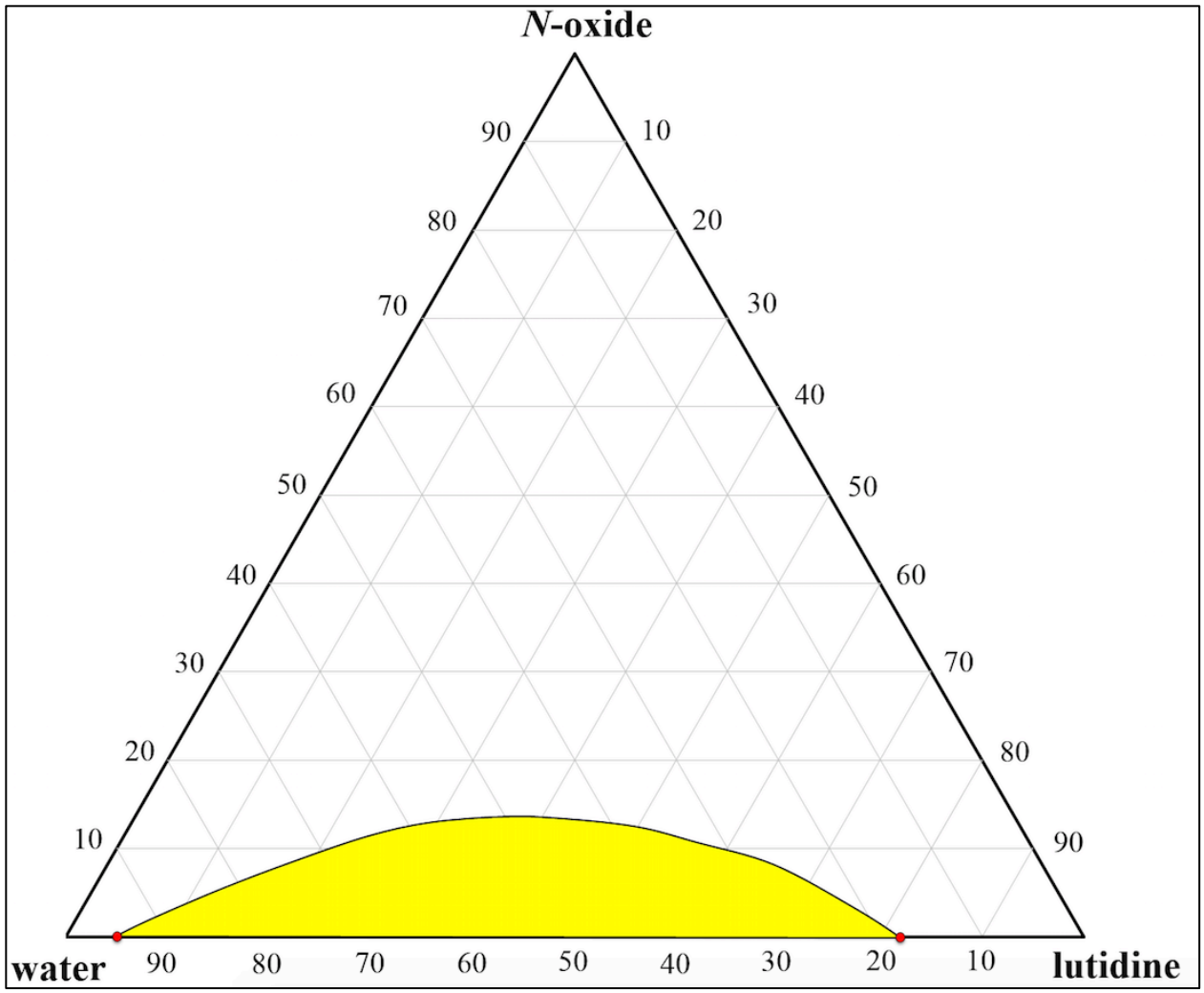

Figure 7. Ternary diagram for the system 2,6-lutidine (lutidine) + 2,6-lutidine-*N*-oxide (*N*-oxide) + water at temperature T = 110 °C showing approximate nature of the binodal curve
Shaded area – Heterogeneous region, Unshaded area – Homogeneous region
For 2,6-lutidine/water system at temperature T = 110 °C, concentration of water in 2,6-lutidine rich phase is 18 wt.% and concentration of 2,6-lutidine in water rich phase is 5 wt.% (Andon *et al*. (1952) (denoted by ● in the figure)
(Reprinted with permission from (Janardanan, Papadaki *et al*. 2017))

4.3.2. FTIR spectra analysis

The total energy possessed by a molecule is a sum of four contributions *i.e.*, electronic energy, vibrational energy, rotational energy and translational energy (Coates 2000). When atoms absorb infrared radiations they vibrate with specific frequencies leading to a change in the dipole

moment of the molecule. The vibrating molecules absorb a portion of the incident energy and the reflected beam is used to construct an absorption spectrum for the sample. The interaction between the sample and the incident beam is a function of the bond angle, bond length and overall structure of the molecules. If the energy absorbed by a sample over any frequency range is recorded then it can provide us with information regarding the molecular backbone and the attached functional groups of the different components. Also, the relationship between the absorption of a molecule and its concentration in the sample is linear (Swinehart 1962).

The Fourier Transform Infrared Spectroscopy (FTIR) used in this research works on a similar principle. It is based on the concept of Attenuated Total Reflectance (ATR) and probes the liquid in the vicinity of the diamond tip (surface measurements). The main advantage of this technique is that it does not disturb the system while taking measurements and generates data instantly. In addition to this, the instrument does not require external temperature controlled devices for collecting and storing samples. Furthermore, the signal-to-noise ratio and energy throughput in an FTIR is larger than regular dispersive instruments (Lewiner, Févotte *et al.* 2001; Lewiner, Klein *et al.* 2001). Owing to these advantages, the FTIR has been used for qualitative and quantitative determination of chemicals in many research areas. For example, Fujiwara *et al.* (2002) studied the crystallization of paracetamol in water using ATR-FTIR and laser backscattering techniques. They concluded that the ATR-FTIR could be used successfully to identify the optimum operating conditions for the crystallization process. Similarly, ATR-FTIR was used to detect the concentrations of methyl esters in biodiesel blends (Oliveira, Montalvão *et al.* 2006). FTIR has also been used to measure the mineral content in coal samples to determine the feasibility of coal in energy production (Painter, Coleman *et al.* 1978). Several other authors have demonstrated the application of the FTIR as an analytical tool (ULBERTH and HAIDER

1992; van de Voort, Ismail *et al.* 1994; Lewiner, Févotte *et al.* 2001; Al−Alawi, van de Voort *et al.* 2005; Swann and Patwardhan 2011).

The *in-situ* FTIR spectrometer used in this work employed mid-infrared frequencies (2500 – 650 cm^{-1}). The probe tip is made of a diamond composite sensor that absorbs in the 2250 – 1950 cm^{-1} frequency region. Hence, the spectral data obtained in this range was not considered during the analysis.

Reference IR spectra for pure solutions of lutidine and *N*-oxide are shown in Figure 8 and 9. The absorption of both the molecules in the 1800 – 650 cm^{-1} frequency region was significant with many characteristic peaks. The vibrational frequencies observed in the lutidine spectra were found to be consistent with the work of Green *et al*. (1970). Also, most of the IR bands for *N*-oxide overlap with lutidine owing to similar molecular structure except the distinctive *N-O* peak at 1248 cm^{-1} (Pineda Solano 2014).

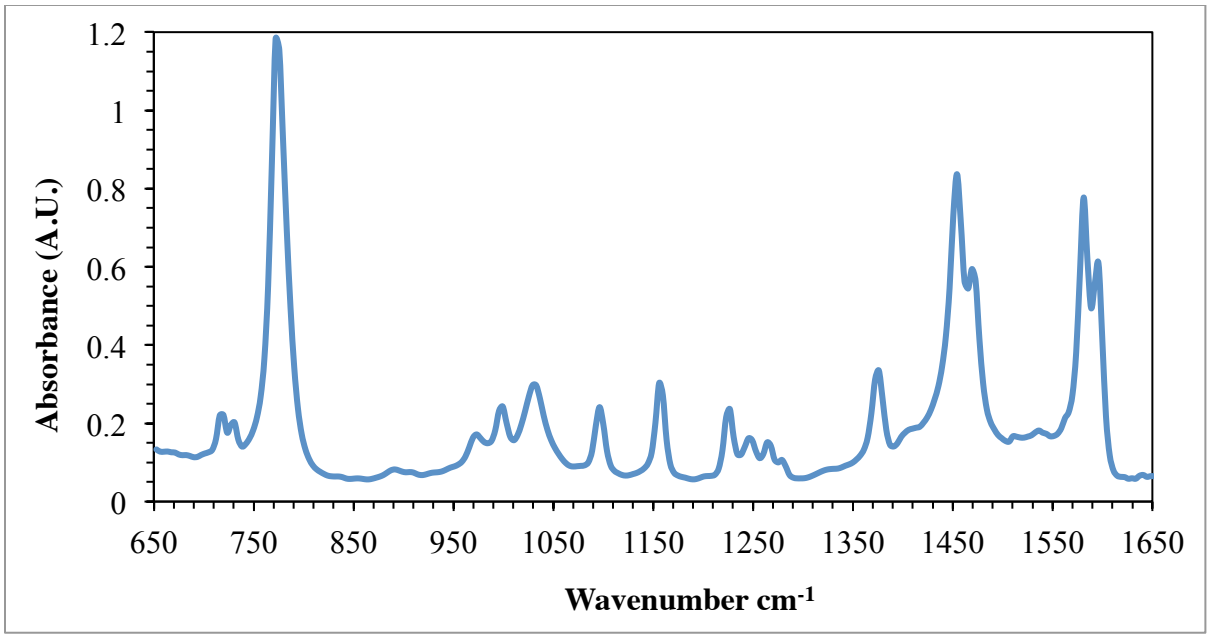

Figure 8. FTIR spectra for 2,6-lutidine solution at temperature $T = 25$ °C
(Reprinted with permission from (Janardanan, Papadaki *et al*. 2017))

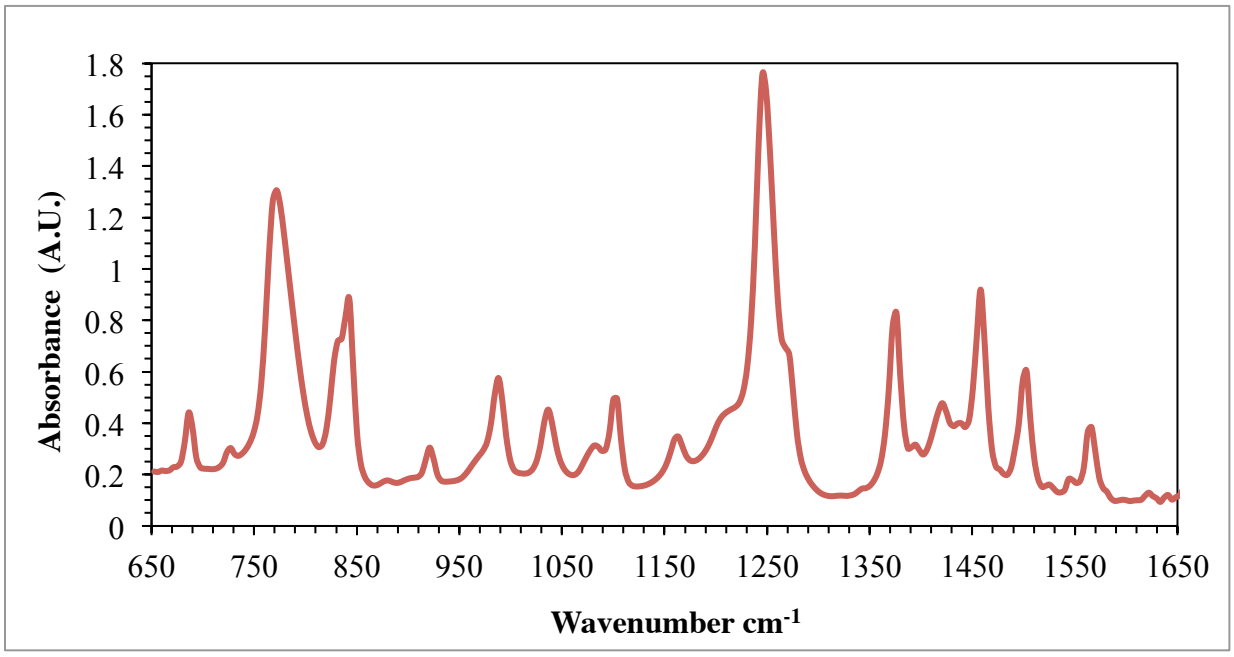

Figure 9. FTIR spectra for 2,6-lutidine-*N*-oxide solution at temperature $T = 25$ °C
(Reprinted with permission from (Janardanan, Papadaki *et al*. 2017))

Prior to testing the ternary mixtures, aqueous solutions of lutidine and *N*-oxide were analyzed using the FTIR probe to understand the effect of water on the individual spectra. The *N*-oxide absorption decreased with increasing water concentration as indicated by the reduction in heights of the *N*-oxide peaks in the spectra (see Figure 10). On the other hand, the absorption area near the 1638 cm^{-1} region showed a gradual rise with increasing dilution. This region corresponds to the absorption in water molecules due to bending vibrations (Brubach, Mermet *et al*. 2005). The FTIR spectra of a lutidine + water system exhibited a slightly different trend with the change in composition. In this case, the infrared bands corresponding to lutidine decreased significantly as the lutidine concentration dropped from 86.29% to 80.72% while a sharp increase was seen in the peak at 1638 cm^{-1}. This anomaly can be ascribed to the liquid-liquid demixing between lutidine and water at this temperature as previously determined by Andon and Cox (1952). Figure 11 highlights the difference between the absorption of homogeneous and heterogeneous mixtures for the two-component system.

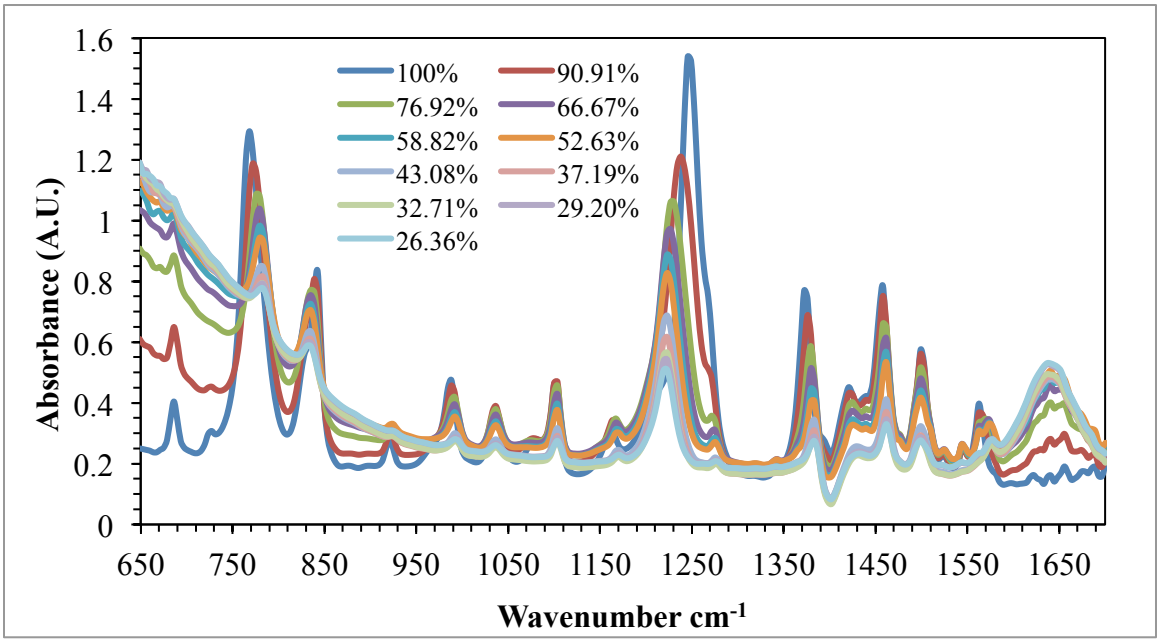

Figure 10. FTIR spectra for mixtures of 2,6-lutidine-*N*-oxide in water at temperature $T = 110$ °C Compositions have been expressed as 2,6-lutidine-*N*-oxide wt.% (Reprinted with permission from (Janardanan, Papadaki *et al*. 2017))

a)

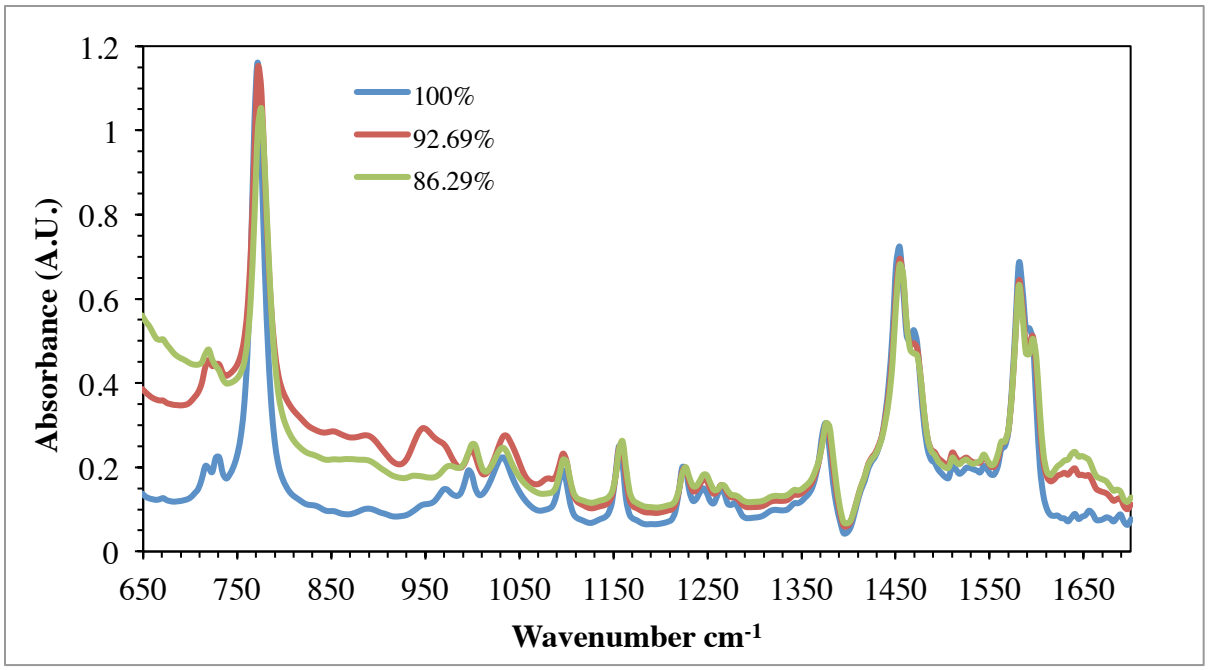

b)

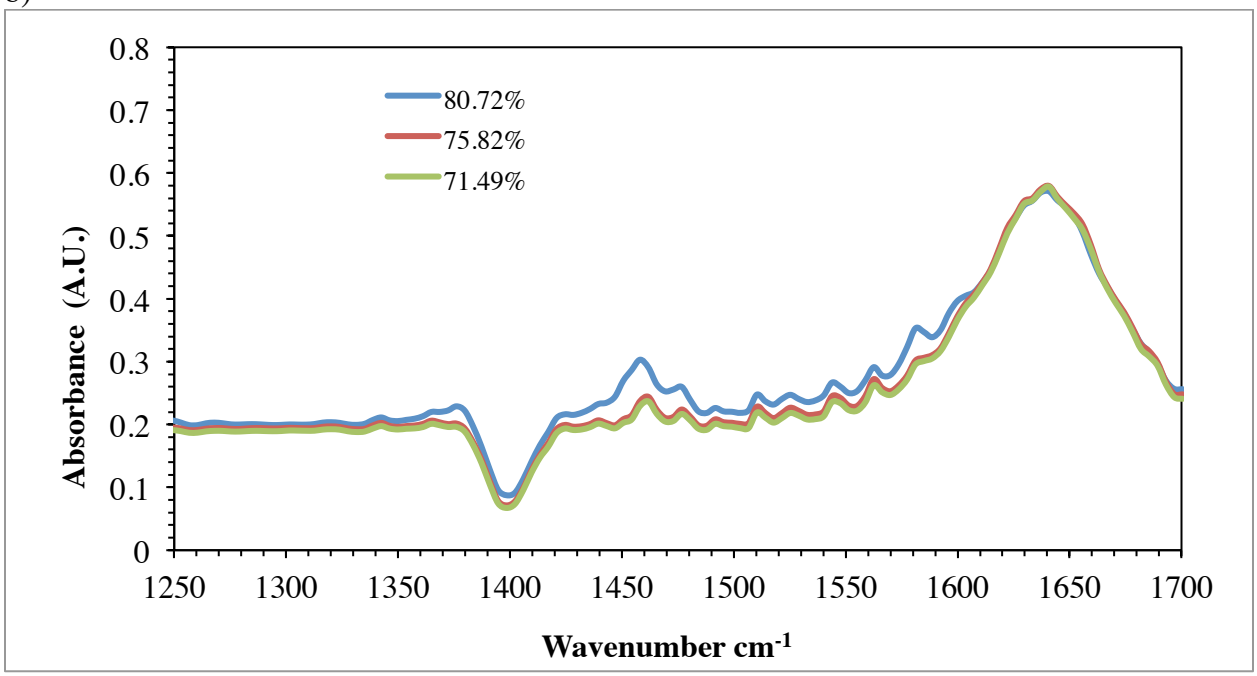

Figure 11. FTIR spectra for mixtures of 2,6-lutidine in water at temperature T = 110 °C a) Homogeneous mixtures; b) Heterogeneous mixtures (Reprinted with permission from (Janardanan, Papadaki *et al*. 2017)) (Compositions have been expressed as 2,6-lutidine wt.%)

The absorption measurements from the dilution of 90/10, 80/20 and 60/40 lutidine + *N*-oxide mixtures are presented in Figure 12, Figure 13 and Figure 14. From Figure 12 and 13, it is clear that the IR spectra of mixtures P5 and Q8 are appreciably different from the other mixtures. In order to substantiate this observation, the peak heights at 772 cm^{-1}, 1451 cm^{-1} and 1638 cm^{-1} were tracked during the process. Table 7 shows the abrupt change in the peak heights between P4 – P5 and Q7 – Q8 that coincides with the previous observation of phase separation in the lutidine + water binary system. As mentioned earlier, these mixtures were examined in the absence of stirring to observe the separated phases. The difference in the absorption characteristics of the mixtures obtained during the dilution of a 60/40 mixture was minor with no steep variations in peak heights at any step. Figure 14 displays the FTIR spectra for some of the mixtures. It can be deduced that the inspected mixtures were homogeneous and did not exhibit any two-phase behavior.

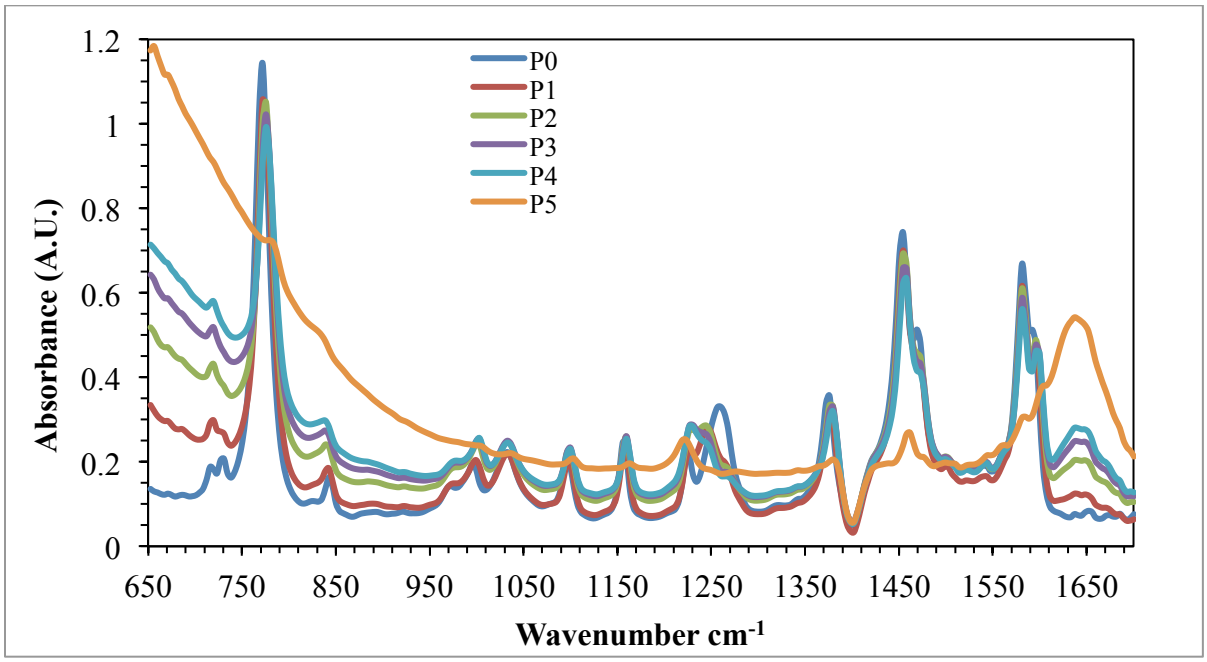

Figure 12. FTIR spectra for ternary mixtures (2,6-lutidine + 2,6-lutidine-*N*-oxide + water) probed during dilution of 90/10 2,6-lutidine + 2,6-lutidine-*N*-oxide mixture at temperature T = 110 °C (Reprinted with permission from (Janardanan, Papadaki *et al*. 2017))

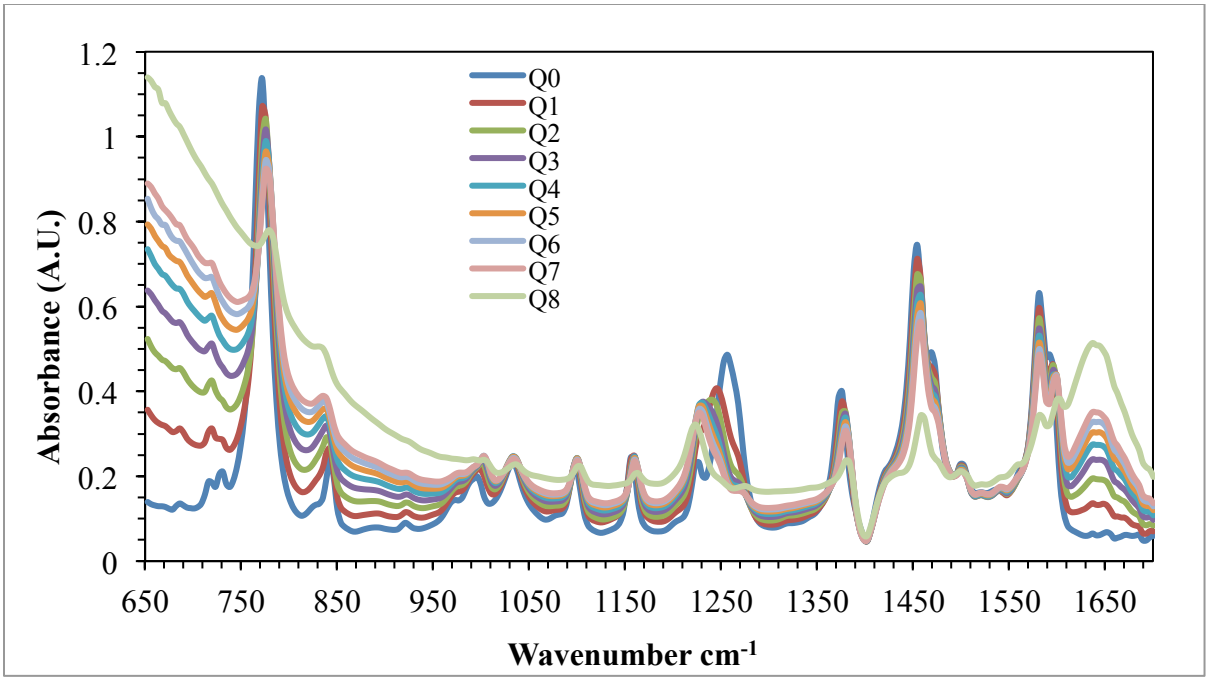

Figure 13. FTIR spectra for ternary mixtures (2,6-lutidine + 2,6-lutidine-*N*-oxide + water) probed during dilution of 80/20 2,6-lutidine + 2,6-lutidine-*N*-oxide mixture at temperature T = 110 °C (Reprinted with permission from (Janardanan, Papadaki *et al*. 2017))

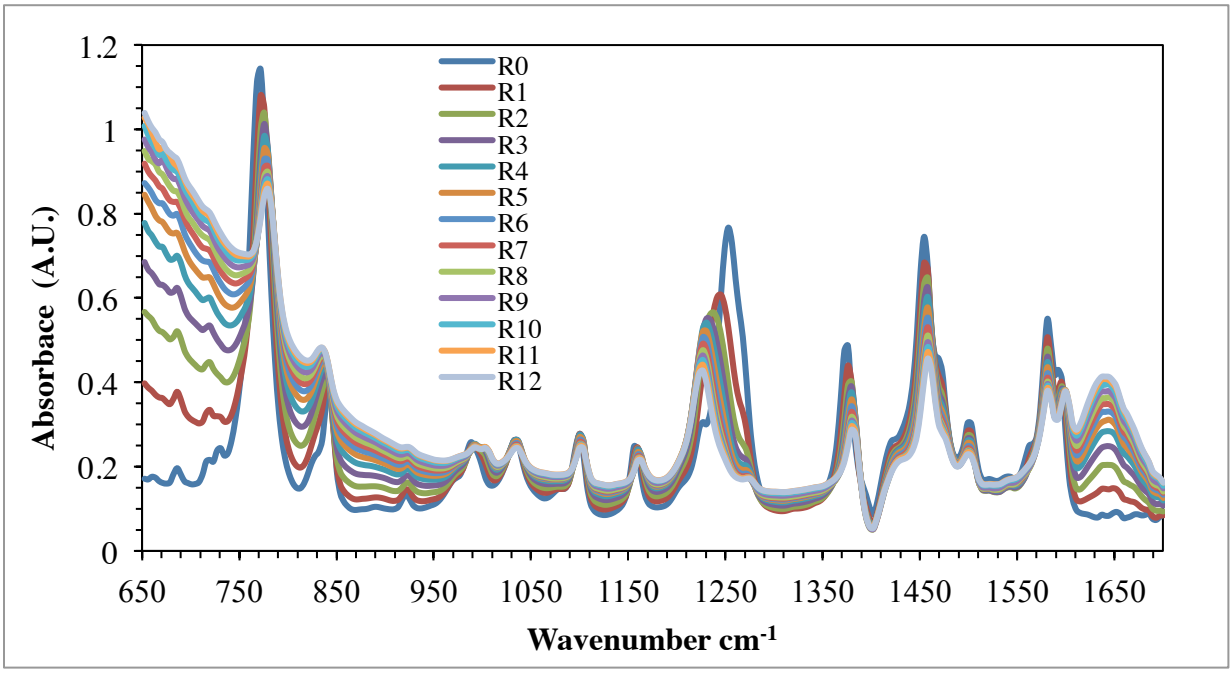

Figure 14. FTIR spectra for ternary mixtures (2,6-lutidine + 2,6-lutidine-*N*-oxide + water) probed during dilution of 60/40 2,6-lutidine + 2,6-lutidine-*N*-oxide mixture at temperature T = 110 °C (Reprinted with permission from (Janardanan, Papadaki *et al*. 2017))

Table 7. Experimental values of average peak heights h for the system 2,6-lutidine + 2,6-lutidine-*N*-oxide + water at temperature T = 110 °C and pressure P = 0.1 MPa (Reprinted with permission from (Janardanan, Papadaki *et al*. 2017))

Mixture	h_1/**A.U.**	Δh_1/**A.U.**	h_2/**A.U.**	Δh_2/**A.U.**	h_3/**A.U.**	Δh_3/**A.U.**
P0	1.15	-	0.74	-	0.08	-
P1	1.06	-0.09	0.70	-0.04	0.12	0.05
P2	1.05	-0.01	0.69	-0.01	0.20	0.08
P3	1.02	-0.03	0.66	-0.03	0.25	0.04
P4	0.99	-0.04	0.62	-0.04	0.27	0.03
P5	0.73	-0.26	0.24	-0.38	0.54	0.27
Q0	1.14	-	0.75	-	0.06	-
Q1	1.07	-0.07	0.71	-0.03	0.14	0.07
Q2	1.04	-0.03	0.68	-0.04	0.19	0.06
Q3	1.02	-0.02	0.64	-0.04	0.24	0.04
Q4	0.99	-0.03	0.61	-0.03	0.27	0.04
Q5	0.96	-0.03	0.58	-0.03	0.30	0.03
Q6	0.94	-0.02	0.55	-0.03	0.33	0.03
Q7	0.92	-0.02	0.53	-0.02	0.35	0.02
Q8	0.77	-0.15	0.30	-0.22	0.51	0.17
R0	1.14	-	0.74	-	0.09	-
R1	1.08	-0.07	0.68	-0.06	0.14	0.06
R2	1.04	-0.04	0.63	-0.05	0.21	0.06
R3	1.01	-0.02	0.59	-0.04	0.25	0.04
R4	0.98	-0.03	0.56	-0.03	0.28	0.04
R5	0.95	-0.03	0.53	-0.03	0.31	0.03
R6	0.93	-0.03	0.50	-0.03	0.33	0.02
R7	0.91	-0.02	0.48	-0.02	0.35	0.02
R8	0.89	-0.02	0.46	-0.02	0.36	0.02
R9	0.88	-0.01	0.44	-0.02	0.38	0.02
R10	0.86	-0.01	0.43	-0.01	0.40	0.02
R11	0.85	-0.01	0.42	-0.01	0.41	0.01
R12	0.84	-0.01	0.40	-0.02	0.41	0.01

Standard uncertainties u are $u(T)$ = 0.002 °C, $u(P)$ = 1 kPa and $u(h)$ = 0.005 A.U.
h_1, h_2, h_3 – absorption peak heights at 772 cm^{-1}, 1451 cm^{-1}, 1638 cm^{-1} respectively

4.4 Conclusions

Various ternary mixtures containing 2,6-lutidine (lutidine), 2,6-lutidine-*N*-oxide (*N*-oxide) and water were investigated in the RC1*e* calorimeter equipped with the FTIR probe. Phase separated mixtures showed a cloudy appearance and a drastic change in the absorption spectra as compared to the homogeneous mixtures. The ternary phase diagram for the system indicates that the 2,6-lutidine, 2,6-lutidine-*N*-oxide and water mixture remains homogeneous over a large composition range. These results suggest that the *N*-oxide concentration will have a major impact on the mixing of the solution during the *N*-oxidation reaction.

5. STUDY OF PHASE BEHAVIOR BETWEEN 2,6-LUTIDINE/2,6-LUTIDINE-*N*-OXIDE/WATER USING MOLECULAR SIMULATIONS[2]

Molecular simulations can be defined as the numerical determination of the thermodynamic, energetic, structural and dynamic properties of chemical aggregates on a digital computer. They utilize theoretical models, which are either empirical or employ parameters derived from *ab initio* techniques. The results are generally compared with the experimental data to determine the exactness of the molecular models and to validate the assumptions made during the simulations. Validated models can be used to study the system at extreme conditions where performing laboratory experiments would be impossible. In other cases, the analysis and interpretation of data obtained from experiments can be done with the help of theoretical models. In general, this technique can be used to generate important process related data in reduced time with limited resources. Molecular simulations find applications in diverse chemical and bimolecular systems including studies involving liquid water, aqueous solution structure, proteins, nucleic acids and membrane dynamics (Beveridge and DiCapua 1989).

Molecular simulations can be broadly classified into 1) Molecular Dynamics (MD) simulations and 2) Monte Carlo (MC) simulations. In addition to this, techniques that incorporate features from both the approaches are also available in this field.

[2] Part of this section is reprinted with permission from 'Janardanan, S., Perez, L. M., & Mannan, M. S. (2018). Study of phase behavior of 2,6-lutidine, 2,6-lutidine-N-oxide and water mixture using UNIQUAC model with interaction parameters determined by molecular simulations. *Thermochimica Acta*', Copyright [2017] by Elsevier.

Molecular Dynamics (MD) provides details regarding the time evolution of any chemical system of atoms and molecules based on their interactions. The simulation considers molecules as set of spherical atoms attached by springs that represent atomic bonds. The energetic interactions operating in the system are given by simple mathematical functions. Mostly, expressions similar to Hooke's law are used to depict bonded interactions while the non-bonded terms are represented by Coulombic and Lennard-Jones potentials (Adcock and McCammon 2006). This technique of mimicking the interatomic interactions using empirical formulas is the core of MD simulations and is termed as the force-field method. The approach neglects the electronic interactions and operates at the atomic level. The total potential energy of the system, which determines the relative stability of the structure (Karplus and Petsko 1990), is the sum of the bonded and non-bonded contributions. After defining the potential energy function, the Newton's equations of motion are solved numerically to predict the fluctuations in structure with respect to time. The methodology for finding solution to these equations is an iterative process, which is based on mathematical algorithms (*e.g.*, Verlet algorithm, Beeman algorithm, velocity Verlet method). The dynamic simulations generate information regarding the motion of individual particles as a function of time, which can be utilized to quantify the system properties including kinetic and thermodynamic data (van Gunsteren and Berendsen 1990; Allen 2004; Adcock and McCammon 2006). Hence, molecular dynamics simulations have found widespread applications in the field of phase equilibrium thermodynamics (Kamath, Lubna *et al.* 2005; Ketko and Potoff 2007; Ren, Zhang *et al.* 2007; Yang and Bae 2008; Oh and Bae 2010). Specifically, they have been useful in predicting the phase behavior of polymer solutions and mixtures containing water, hydrocarbons, alcohols, chlorides.

On the other hand, the Monte Carlo (MC) method is a sampling technique aimed at analyzing the various configurations of any molecular ensemble with the purpose of identifying different possible stable and metastable states for the system (Dove 2008). In the field of computational science, the Metropolis version of this algorithm is common. In this method, several conformations of the system are generated by randomly moving the molecules and measuring the energy change (ΔE). A negative value of ΔE indicates that the conformation is energetically favorable and can be accepted. On the contrary, if the value of ΔE is positive then the selection is based on comparison between a random number and the Boltzmann probability $exp(-\Delta E/k_bT)$ of the movement. If the Boltzmann probability of the move is larger than the random number, then the new configuration is accepted; else the system is returned to its original state. In this way, large numbers of samples are investigated to ensure that the procedure maintains thermodynamic consistency. A simple arithmetic average of a property from individual accepted configurations provides the correct thermodynamically weighted value for the quantity. This approach has been applied for determining structural and thermodynamic properties of condensed phase systems.

In this study, a combination of both these techniques was utilized to estimate the binary interaction energies for the various molecular pairs in the three-component system. The molecular simulation details have been provided in subsection 5.1.3. The results were incorporated in a thermodynamic model (UNIQUAC) to estimate the biphasic compositions for the phase separated mixture and study the impact of temperature on the phase diagram. The UNIQUAC activity coefficient model has been successful in predicting the vapor-liquid and liquid-liquid equilibrium in ternary solutions with satisfactory accuracy. The model equations describe the molecular interactions in any system in terms of adjustable parameters that depend

on the interaction energies between the component pairs. The model description has been included in subsection 5.1.1. Generally, the parameters are derived empirically by fitting the equations to data obtained from phase equilibrium experiments. However, computational techniques have been used recently to calculate these parameters to reduce the dependence of these models on experimental data. For example, Sum and Sandler (1999) used *ab intio* quantum mechanics to create molecular clusters representing several binary aqueous systems and computed the interaction energies between like and unlike pairs. These values were used to predict the adjustable parameters, which were used to construct the VLE for these systems. Similarly, an indirect method was used to relate the UNIQUAC parameters to the solvation energies, which were calculated using quantum mechanical solvation models (Lin and Sandler 1999). In general, it is evident that the energy parameters used in the UNIQUAC equation have sound theoretical basis. In addition to this, the UNIQUAC model also depends on size and shape parameters of individual molecules. For this work, *ab initio* quantum mechanics was used to determine the molecular parameters for *N*-oxide, as relevant information was not available in literature. The approach and simulation procedure has been incorporated in subsection 5.1.2. All quantum chemical calculations were performed in Gaussian 09 (Frisch, Trucks *et al.* 2009). The results from the simulations and the application of the UNIQUAC model have been discussed in subsection 5.2. The conclusions from this work have been listed in subsection 5.3.

5.1. Theory and Methodology

5.1.1. UNIQUAC Model

The liquid-liquid equilibrium in any ternary mixture can be described by the isoactivity criterion (Sørensen, Magnussen *et al.* 1979), which equates the product of the activity coefficient and mole fraction of any species in the two phases.

$$(x_i\gamma_i)^1 = (x_i\gamma_i)^2 \qquad (3)$$

$$\sum x_i^1 = \sum x_i^2 = 1 \qquad (4)$$

Where, x_i^1 and x_i^2 are mole fractions of component *i* in phase 1 and phase 2, while γ_i^1 and γ_i^2 are the activity coefficients of component *i* in the respective phases. In order to estimate the phase compositions, it is necessary to calculate the activity coefficients of the various species present in the mixture. Thermodynamic models represent the activity coefficients in terms of empirical or semi-empirical expressions, which incorporate molecular and intermolecular parameters. Out of these models, the ones that are based on the local composition concept of Wilson (1964) have more theoretical basis as compared to others. The universal quasi-chemical (UNIQUAC) model of Abraham and Prausnitz (1975) belongs to this category. It is based on the quasi-chemical theory of Guggenheim (1952) and is applicable to non-random mixtures containing molecules of different sizes. The activity coefficient expression includes two parts, the first part accounts for the difference in the size and shape of the molecules while the second part incorporates the intermolecular interactions.

$$\ln \gamma_i = \ln \frac{\phi_i}{x_i} + 5q_i \ln \frac{\theta_i}{\phi_i} + l_i - \frac{\phi_i}{x_i} \sum_j x_j l_j + q_i \left[1 - \ln \left(\sum_j \theta_j \tau_{ji} \right) - \sum_j \left(\frac{\theta_j \tau_{ij}}{\sum_k \theta_k \tau_{kj}} \right) \right] \quad (5)$$

Here, the segment fraction (ϕ_i) and area fraction (θ_i) are given by

$$\phi_i = \frac{x_i r_i}{\sum_j x_j r_j} \quad (6)$$

$$\theta_i = \frac{x_i q_i}{\sum_j x_j q_j} \quad (7)$$

$$l_i = \left(\frac{z}{2} \right) (r_i - q_i) - r_i + 1 \quad (8)$$

The surface area and volume parameters for individual components are represented by r and q. z denotes the coordination number for every species in the mixture and has a fixed value (10). The binary adjustable parameters (τ_{ij}) describe the energetic interactions between the component pairs. The following expression can be used to calculate these parameters.

$$\tau_{ij} = \exp \left(\frac{u_{jj} - u_{ij}}{RT} \right) \quad (9)$$

In the above equation, the u_{ii}, u_{jj} correspond to the interaction energy between like and unlike molecules.

5.1.2. Estimation of molecular volume and surface area for N-oxide using GEPOL algorithm and Polarizable Continuum Model

The structural parameters included in the UNIQUAC model can be directly related to the van der Waals volume and surface area of any molecule through the Bondi's (1964) equation. The volume and surface area of a compound can be obtained from the molecular surface. The simplest description of the molecular surface is based on a set of overlapping spheres centered on atoms or group of atoms forming the molecule. This is termed as the van der Waals (vdW) surface. Similarly, molecular surface can also be defined based on Lee and Richards concept of Solvent Accessible Surface (SAS). In this method, the surface generated by the center of the solvent probe sphere that is rolling on the vdW surface of a molecule is considered for computations (Connolly 1983). However, Richards Solvent Excluded Surface (SES) is the most frequently used method for characterizing molecular surfaces. This surface is a combination of two parts, the contact surface and reentrant surface. Contact surface is the part of the vdW surface of each atom that can be accessed by a rigid probe sphere while reentrant surface is the inward-facing part of the probe sphere which contacts more than one atom (Richards 1977).

GEnerating POLyhedra (GEPOL) algorithm of Nilson *et al.* (1990) has been commonly used for construction of vdW, SAS and SES type surfaces for various chemical systems. When compared to other surface-building methods the algorithm is more accurate and takes less computational time. In the first step the algorithm generates the van der Waal surface by creating spheres around each atom of the molecule based on the user defined input radii. After generating the vdW surface, the program identifies the region on the surface that is inaccessible to the solvent.

This process involves calculation of the distances and overlap angles between the spherical pairs. Once the spherical ensemble is created, each sphere is partitioned into triangular tesserae forming a pentakisdodecahedron and the triangles in the intersection volume of the spheres are deleted using a geometrical procedure. The total surface area of the resulting surface is a summation of the areas of all the remaining triangles while the total volume is the summation of the solid volumes made by the triangular surfaces with the origin. Details regarding the methodology employed in the algorithm have been discussed elsewhere (Pascual−Ahuir, Silla *et al.* 1987; Pascual−Ahuir and Silla 1990; Silla, Tunon *et al.* 1991; Pascual−ahuir, Silla *et al.* 1994)

GEPOL finds widespread application in solvation models wherein the solute-solvent interactions are studied by creating a solute cavity in the solvent continuum. The cavity surface constructed by GEPOL is discretized into point charges polarizing the dielectric medium (solvent), which in turn generates a charge distribution on the solute-solvent boundary. *Polarizable Continuum Model* (PCM) of Tomasi (Miertuš, Scrocco *et al.* 1981) is an example of a continuum solvation procedure that incorporates GEPOL for building the solute cavity. In the present work, the PCM-GEPOL procedure was utilized to construct the structure of the *N*-oxide molecule and estimate its area and volume. Before employing the procedure, the *N*-oxide structure was optimized to get a minimum energy configuration using Density Functional Theory with B3LYP functional (Lee, Yang *et al.* 1988; Becke 1993) at 6-311++G(3d,2p) basis set. The optimized structure was used as the solute in the PCM calculations, which utilized Bondi's atomic radii for generation of vdW spheres. The program multiplies the radii of each sphere by a scale factor (*alpha*) to account for the difference in the dielectric of the first solvation layer and the bulk solution in free energy

calculations (Sahandzhieva, Tuma *et al.* 2006). *Alpha* was set to '1' since the objective was to compute the cavity.

5.1.3. Molecular simulation for determination of binary interaction energies

Blends module of Materials Studio (version 4.2) was used to conduct molecular dynamics simulations for determining the energy parameters. The program predicts the binding energy of binary pairs based on a Monte Carlo sampling technique (Fan 1992). In this method, several configurations of a molecular pair are generated such that the van der Waals surfaces of the two molecules are oriented according to the excluded volume constraints approach (Blanco 1991). The Metropolis sampling algorithm is used to accept the configurations with appropriate energetics and the pairwise interaction energy is calculated by averaging all accepted configurations using the Boltzmann factor. Blends computes the energy of a molecular system based on the force-field method. For this study, COMPASS (Condensed Phase Optimized Molecular Potentials for Atomistic Simulation Studies) force-field (Sun 1998) was selected to perform the calculations. COMPASS, an extended version of CFF series, employs parameters derived from condensed phase data. It has been developed for studying the structure and dynamics of organic, inorganic and polymer molecules. The functional form of this force field relates the total energy of a molecular ensemble to the valence and nonbond interaction terms. The valence terms include the internal coordinates of bond, angle, torsional and out-of-plane angle along with combinations of two or three internal coordinates like bond-bond, bond-angle and angle-torsion-angle. On the other hand, the non-bond interaction terms comprise of contributions arising from the electrostatic and vdW type forces between atoms. A coulombic

function based on partial atomic charges is used to describe the electrostatic interaction while the vdW term is represented by a LJ-9-6 function.

The steps involved in obtaining the interaction energies using the simulation software are as follows.

(I) 2,6-lutidine, 2,6-lutidine-*N*-oxide, water structures were constructed by using sketching tools in Materials Studio.

(II) The structures were subjected to the energy minimization procedure to obtain the optimized geometry.

(III) The optimized structures were used in the Blends module and the following parameters were set – number of energy samples = 10^7, number of cluster samples = 10^4, iterations per cluster = 20.

The Blends simulations were conducted for two sets of nitrogen and oxygen partial charges for every pair as shown in Table 8. Set 1 was determined through *ab initio* calculations performed on each of the dimer (2,6-lutidine/water, 2,6-lutidine-*N*-oxide/water, 2,6-lutidine/2,6-lutidine-*N*-oxide). The electrostatic potential energy surfaces (ESP) for the dimers obtained through energy minimization using M062X/6-311++g(3d,2p) level (Zhao and Truhlar 2008)were analyzed using the CHELPG methodology (Breneman and Wiberg 1990) to derive the partial charges. Figure 15 displays the final structure of the dimers obtained after the optimization process. It must be noted that the most stable conformers for the pairs were considered for deriving the ESP charges. The second set of partial charges (set 2) was selected heuristically in order to reproduce the experimental binodal curve predicted by Janardanan et al. (2017).

Table 8. Partial charges (q_i) assigned to atoms during molecular simulations (Reprinted with permission from ((Janardanan, Perez *et al*. 2018)))

Set	Dimer	Site	Charge (q_i)
1	$C_7H_9N - H_2O$	N O	-0.52 -0.73
	$C_7H_9N^*O^* - H_2O$	N* O* O	0.15 -0.49 -0.77
	$C_7H_9N - C_7H_9N^*O^*$	N N* O*	-0.65 0.17 -0.50
2	$C_7H_9N - H_2O$	N O	-0.60 -0.61
	$C_7H_9N^*O^* - H_2O$	N* O* O	0.18 -0.50 -0.74
	$C_7H_9N - C_7H_9N^*O^*$	N N* O*	-0.40 0.18 -0.50

a)

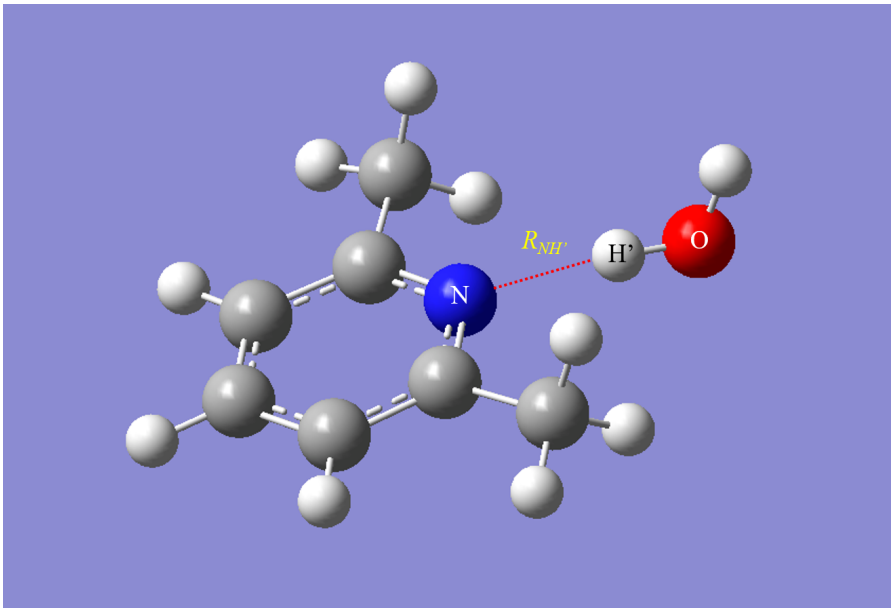

$R_{NH'}$ (Non-bonded distance between nitrogen and hydrogen) = 1.9092 A^o

Figure 15. 3D structures of dimers obtained from *ab initio* calculations
a) 2,6-lutidine/water, b) 2,6-lutidine-*N*-oxide/water, c) 2,6-lutidine/2,6-lutidine-*N*-oxide
(Reprinted with permission from (Janardanan, Perez *et al.* 2018))

b)

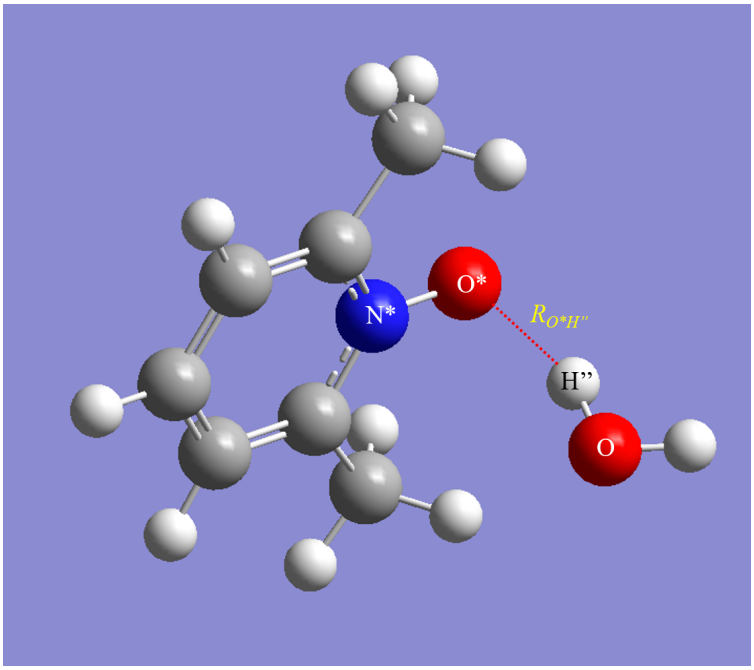

$R_{O*H''}$ (Non-bonded distance between oxygen and hydrogen) = 1.8091 A^{o}

c)

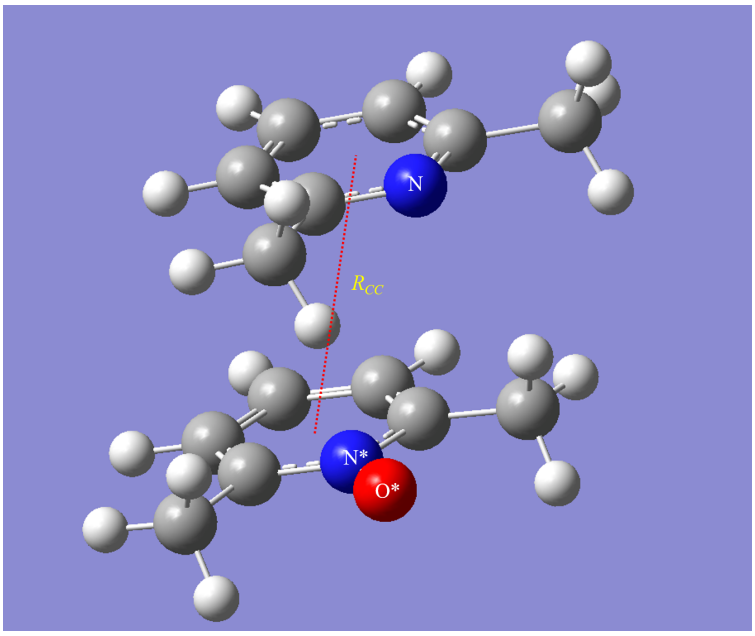

R_{CC} (Distance between ring centers) = 3.5848 A^{o}

Figure 15. Continued

5.2. Results and Discussion

5.2.1. Binary interaction parameters and ternary diagrams

Table 9 shows the molecular volume and surface area for 2,6-lutidine-*N*-oxide obtained using the GEPOL algorithm. These values were used to evaluate the volume (*r*) and surface area (*q*) parameters for the compound based on the following equations.

$$r_{est} = \frac{V \times N_{av}}{V_{ws}} \tag{10}$$

$$q_{est} = \frac{A \times N_{av}}{A_{ws}} \tag{11}$$

In Eqs. (10) and (11), V_{ws} and A_{ws} are the standard segment volume and standard segment area and 'N_{av}' is the Avogadro's constant. The numerical values for V_{ws} (15.17 cm^3/mol) and A_{ws} (2.5 x 10^9 cm^2/mol) were taken from literature. Table 10 displays the structural parameters for the three compounds in the current system. The *r* and *q* values for 2,6-lutidine and water were extracted from ASPEN (Aspen Plus Version 8.2) which uses group contribution method for calculating the parameters.

Table 9. GEPOL volume and surface area for 2,6-lutidine-*N*-oxide
(Reprinted with permission from (Janardanan, Perez *et al.* 2018))

Volume (V) ($Å^3$)	Area (A) ($Å^2$)
119.886	156.128

Table 10. UNIQUAC volume (r) and surface area (q) structural parameters for the system (Reprinted with permission from (Janardanan, Perez *et al.* 2018))

Compound	r	q
Water	0.9200	1.4000
2,6-lutidine	4.4693	3.4384
2,6-lutidine-*N*-oxide	4.7598	3.7614

The interaction energies predicted by Blends module have been incorporated in Table 11 along with the binary parameters estimated using Eqs. (9). Based on the results, certain observations can be made regarding the intermolecular behavior in the two-component systems. For example, it is clear that the strength of interaction between 2,6-lutidine/water (u_{12}) is lower than the 2,6-lutidine/2,6-lutidine (u_{22}) dimer in the aqueous mixture. If we compare these values to gas phase interaction energies computed at M062X/6-311++g(3d,2p) level, we find that the trend is reversed (see Table 12). This indicates that the strength of hydrogen bonding between lutidine/water pair reduces as we go from gas phase to aqueous phase, which is similar to the observations made by Malaspina et al. (2002) for aqueous pyridine systems. An identical relationship exists between the 2,6-lutidine-*N*-oxide/water (u_{13}) and 2,6-lutidine-*N*-oxide/2,6-lutidine-*N*-oxide (u_{33}) dimer pair as shown in Table 11 and 12.

Table 11. Interaction energies[a] (Δu) and binary parameters (τ_{ij}) for water (1) + 2,6-lutidine + 2,6-lutidine-*N*-oxide (3) system calculated by molecular simulations (Reprinted with permission from (Janardanan, Perez *et al.* 2018))

	Δu_{12} (J/mole)	Δu_{21} (J/mole)	Δu_{13} (J/mole)	Δu_{31} (J/mole)	Δu_{23} (J/mole)	Δu_{32} (J/mole)	T (°C)
Set 1	-2858.76	98.91	-4546.54	3384.02	-2943.44	2198.52	110
Set 2	-3771.58	1420.89	-5058.37	3414.02	-3866.14	2272.00	110
Set 1	-2850.73	139.62	-4590.73	3523.35	-3005.37	2271.28	100
Set 2	-3798.24	1460.72	-5104.90	3548.87	-3969.74	2339.27	100
Set 1	-2867.92	53.47	-4500.14	3211.22	-2875.66	2105.97	125
Set 2	-3756.77	1352.56	-4987.50	3250.13	-3786.48	2145.72	125

Table 11. Continued

	τ_{12}	τ_{21}	τ_{13}	τ_{31}	τ_{23}	τ_{32}	T (°C)
Set 1	0.4076	1.0315	0.2399	2.8929	0.3969	1.9940	110
Set 2	0.3060	1.5621	0.2043	2.9203	0.2971	2.0405	
Set 3	0.3385[b]	1.592[b]	0.2043	2.9203	0.2971	2.0405	
Set 1	0.4086	1.0448	0.2366	3.0223	0.3892	2.0401	100
Set 2	0.3035	1.5817	0.2013	3.0466	0.2876	2.0841	
Set 3	0.3676[b]	1.5195[b]	0.2013	3.0466	0.2876	2.0841	
Set 1	0.4064	1.0169	0.2434	2.7402	0.4054	1.9369	125
Set 2	0.3074	1.5289	0.2089	2.7739	0.3046	1.9612	
Set 3	0.3170[b]	1.6585[b]	0.2089	2.7739	0.3046	1.9612	

[a] $\Delta u_{ij} = u_{jj} - u_{ij}$
[b] Calculated based on Eqs. (12)

Table 12. Gas phase interaction energies[a] (u) for 2,6-lutidine/water, 2,6-lutidine-*N*-oxide/water, 2,6-lutidine dimer (Parallel arrangement) and 2,6-lutidine-*N*-oxide dimer (Parallel arrangement) computed at M062X/6-311++g(3d,2p) level of theory (Reprinted with permission from (Janardanan, Perez *et al.* 2018))

u_{12} (kJ/mole)	u_{22} (kJ/mole)	u_{13} (kJ/mole)	u_{33} (kJ/mole)
-33.64	-27.03	-36.36	-29.96

[a]Basis Set Superposition Error was included in the calculations

Both the structural and energy parameters were used to solve Eqs. (3) and (4) to determine the biphasic compositions for the ternary system. The resulting tie lines and binodal curve for the mixture at 110 ^{o}C have been shown in Figure 16. The figure also includes the experimental data obtained by Janardanan et al. (2017). As we can see, the binodal curve generated by set 1 shows maximum deviation from the experimental results as compared to the other two sets. On the other hand, set 2 could predict the phase behavior with more accuracy as indicated by the reduction in the two-phase region of the ternary diagram. A further decrease in the error between the model predictions and the experimental measurements was obtained by considering a third

set (set 3) of binary parameters. In this case, the 2,6-lutidine/water interaction parameters (τ_{12}, τ_{21}) were calculated according to the following expression proposed by Saenz-Noval (2011),

$$\tau_{ij} = \exp\left(A_{ij} + \frac{B_{ij}}{T} + C_{ij}\ln(T) + D_{ij}T \right) \quad (12)$$

For i = water, j = lutidine

A_{ij} = 352.95 A_{ji} = 4.45

B_{ij} = -13533.83 B_{ji} = 1801.29

C_{ij} = -57.74 C_{ji} = -2.42

D_{ij} = 0.0646 D_{ji} = 0.0149

Set 1

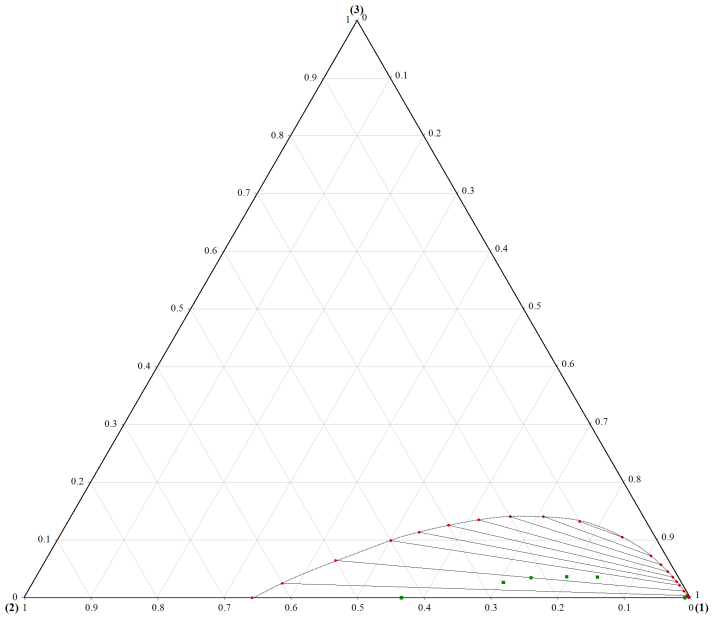

Figure 16. Phase diagrams for the system (water (1) + 2,6-lutidine + 2,6-lutidine-*N*-oxide (3) at 110 ^{o}C): Red dots correspond to the compositions predicted by the UNIQUAC model; Green squares represent the points inside the binodal curve based on experimental data (Reprinted with permission from (Janardanan, Perez *et al.* 2018) and (Janardanan, Papadaki *et al.* 2017)); (ProSim software was used to construct the ternary diagram)

Set 2

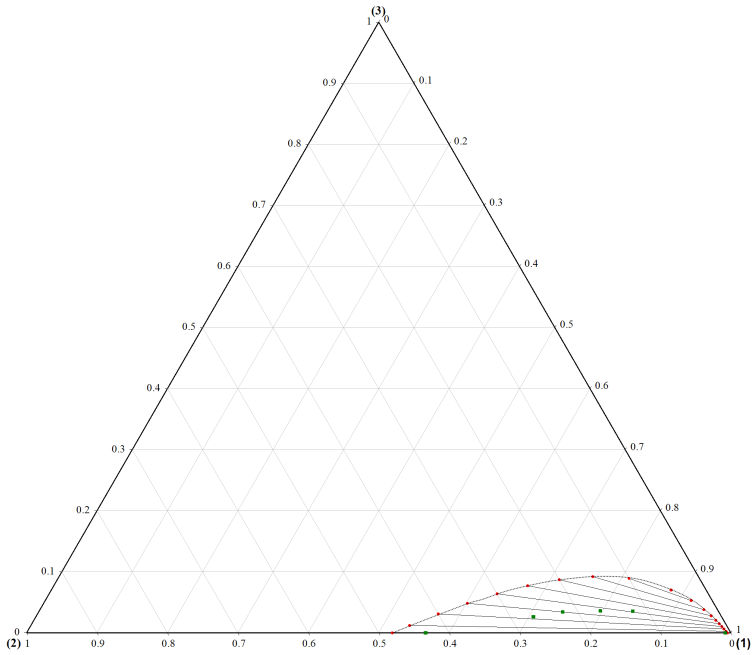

Set 3

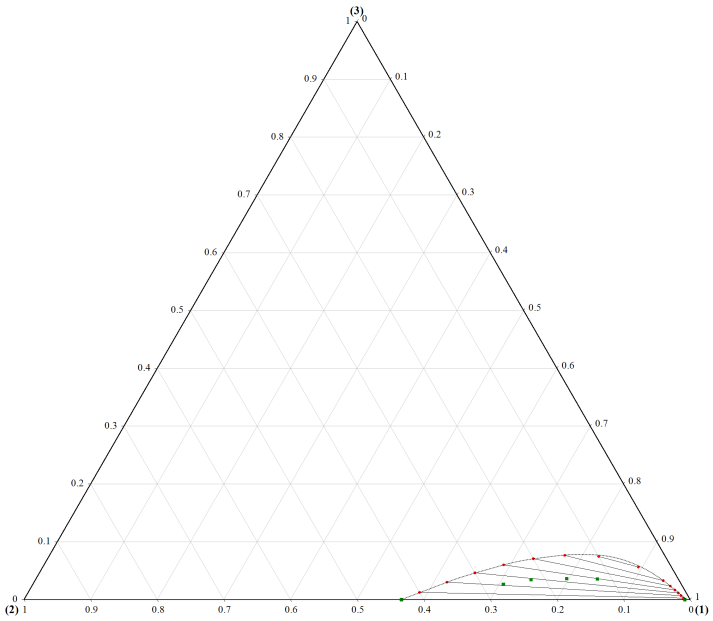

Figure 16. Continued

This expression was based on the regression of experimental data for the binary system. The interaction parameters for other two molecular pairs were left unchanged from set 2. This approach was adopted since the ternary LLE predictions are more sensitive to the binary parameters of the pair that exhibits liquid liquid phase separation (Prausnitz 1980). It can be seen that the binodal curve predicted by this parameter set shows reasonable agreement with the experimental results. In general, all the three sets could predict the 'type 1' (Treybal classification) (Treybal 1963) phase behavior of the system, wherein one binary pair is immiscible while others are miscible. Also, the phase diagram suggests that the binodal curve for the mixture is asymmetric since the composition of the aqueous phase does not change significantly as compared to the organic phase for different equilibrium tie lines. In addition to this, it can be inferred that the plait point composition for the three-component system lies closer to the aqueous phase composition obtained during the lutidine/water split at the same temperature.

In the next step, the partial charge sets were used to generate interaction parameters at two other temperatures. These simulations were done with an objective of studying the effect of temperature on the ternary diagram. Figure 17 and 18 shows the phase diagram for the three component system at temperature T = 125 ^{o}C and T =100 ^{o}C. From the figures, it is evident that the two-phase region for the system decreases at T = 100 ^{o}C and increases at T = 125 ^{o}C for all the parameter sets. Though, the simulation results could not be verified due to lack of experimental data, it could be assumed that the predictions made by the model provide a reasonable estimate of the phase compositions at the considered temperatures. Also, the trend followed by the plait point of the system with temperature is in accordance with the observations

made by Janardanan et al. (2017). The result implies that the amount of 2,6-lutidine-*N*-oxide required for maintaining homogeneity in the ternary mixture increases with temperature.

Though the results are reasonable, the authors would like to discuss some of the assumptions involved in the proposed methodology. The UNIQUAC is based on the local composition concept. The local composition equations are not consistent with the model from which they were derived (Flemr 1976; McDermott and Ashton 1977). Hence, it can be argued that UNIQUAC is empirical in nature and may not be suitable for theoretical modeling. Therefore, the applicability of the current approach for LLE predictions in other systems cannot be guaranteed. Nonetheless, several papers have treated the equations as semi-empirical for the purposes of equilibrium calculations (Jónsd, Rasmussen *et al.* 1994; Jónsdóttir, Klein *et al.* 1996; Sum and Sandler 1999). Secondly, the model neglects the ternary interactions that exist in a three-component mixture. The positive deviations between the simulation results and the experimental data can be attributed to this limitation. Though the inclusion of ternary parameters to the model have been suggested by previous publications (Cha and Prausnitz 1985; Nagata and Usui 1989), the current capabilities in the field of molecular simulations do not allow for accurate predictions of three body interactions in condensed phase systems.

Set 1

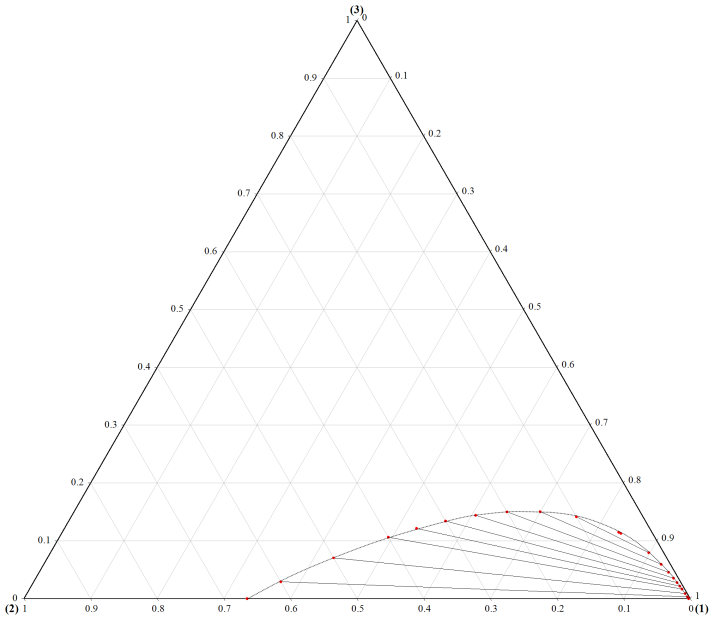

Set 2

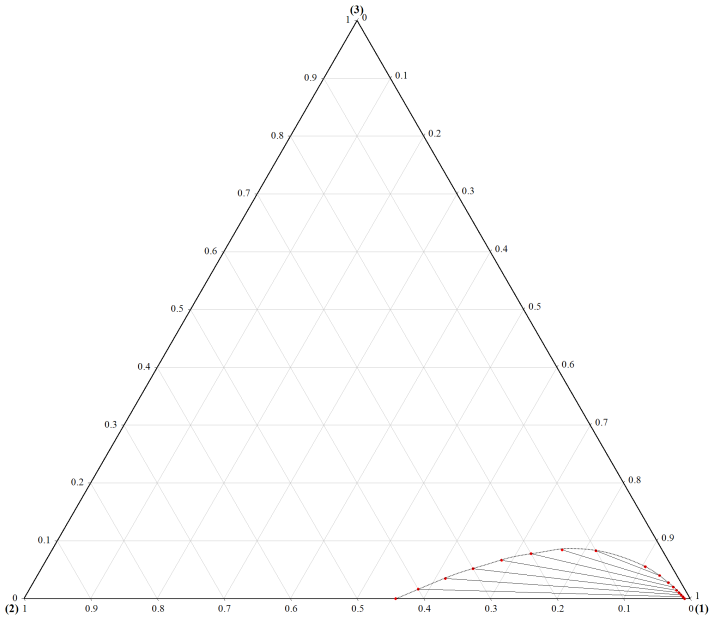

Figure 17. Phase diagrams for the system (water (1) + 2,6-lutidine + 2,6-lutidine-*N*-oxide (3) at 125 ^{o}C): Red dots correspond to the compositions predicted by the UNIQUAC model; Green squares represent the points inside the binodal curve based on experimental data (Reprinted with permission from (Janardanan, Perez *et al.* 2018) and (Janardanan, Papadaki *et al.* 2017)); (ProSim software was used to construct the ternary diagram)

Set 3

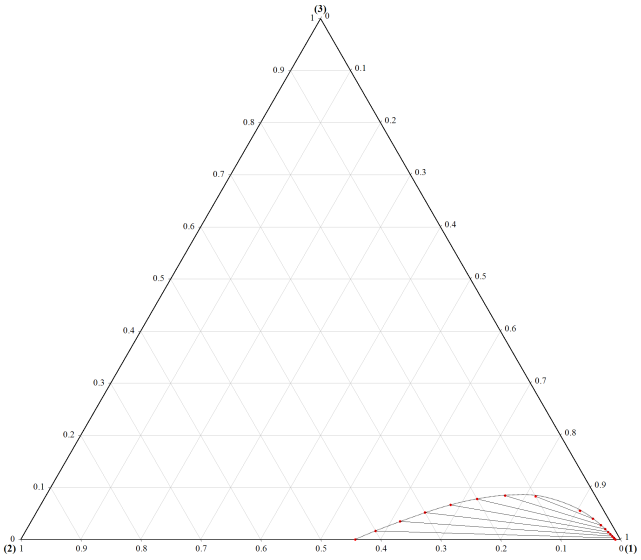

Figure 17. Continued

Set 1

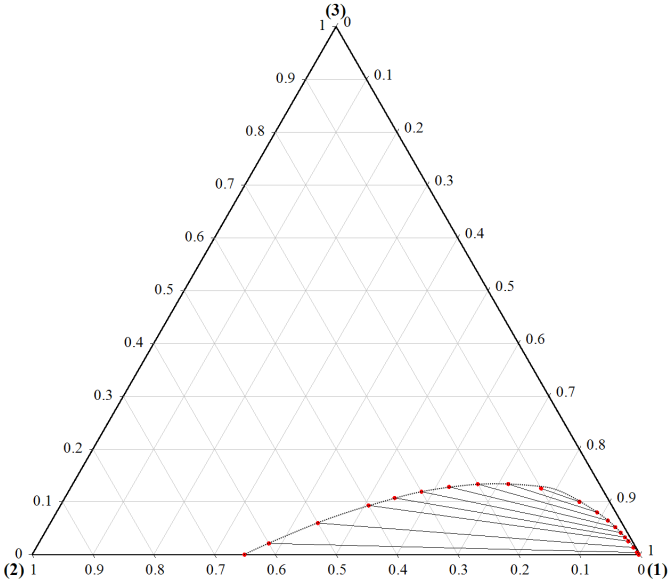

Figure 18. Phase diagrams for the system (water (1) + 2,6-lutidine + 2,6-lutidine-*N*-oxide (3) at 100 ^{o}C): Red dots correspond to the compositions predicted by the UNIQUAC model; Green squares represent the points inside the binodal curve based on experimental data (Reprinted with permission from (Janardanan, Perez *et al.* 2018) and (Janardanan, Papadaki *et al.* 2017)); (ProSim software was used to construct the ternary diagram)

Set 2

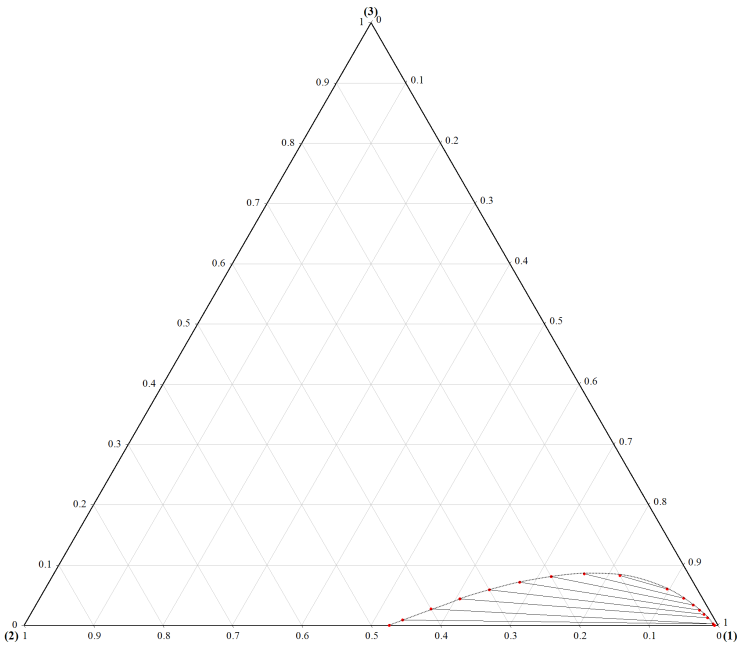

Set 3

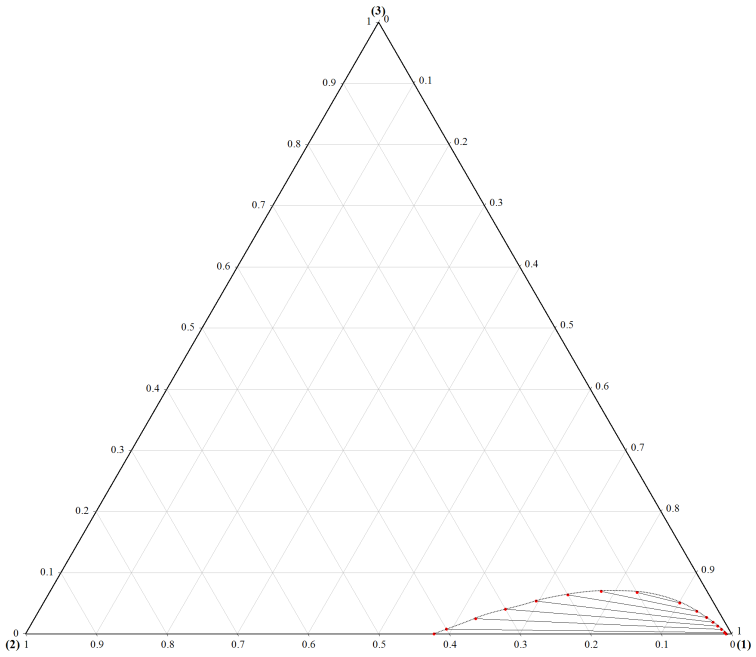

Figure 18. Continued

5.2.2. Parameterization of partial charges for the binary systems

Partial atomic charges play an important role in determining the reactivity of molecules in any environment. The electrostatic interactions that contribute significantly to the intermolecular forces are governed by the partial charges assigned to the atoms. A particularly successful approach is to optimize the charges based on experimental physicochemical and equilibrium data for pure liquids and mixtures to develop parameter sets, which could provide reliable predictions (Jorgensen and McDonald 1998; Kamath, Lubna *et al.* 2005; Ketko and Potoff 2007). A similar methodology was adopted in this work. Before optimizing the individual structures of 2,6-lutidine, 2,6-lutidine-*N*-oxide and water, the partial charges were assigned based on the COMPASS forcefield. In the following step, the partial charges on the nitrogen and oxygen atoms were reassigned according to Table 8. Consequently, the charges on the *ortho*-carbons of lutidine and *N*-oxide were modified to maintain charge neutrality. Similarly, the hydrogen partial charges in water were altered to balance the negative charge on oxygen. This approach is slightly unconventional as compared to the normal parameterization procedure wherein the partial charges on all the atoms are optimized. However, previous publications (Ketko and Potoff 2007) have established the non-uniqueness of the forcefield parameters and the current method was successful in generating interaction energies, which could reproduce the LLE curve with reasonable accuracy.

The first set of partial charges (set 1) was obtained through the CHELPG analysis, which derives the partial charges based on the molecular electrostatic potential. This method has been found to be relatively more accurate as compared to some of the other population techniques (Das, Sahu

et al. 2017). Also, the M062X/6-311++g(3d,2p) level of theory was used to conduct the *ab initio* calculations. Here, we would like to mention that a variety of *ab initio* methods (*e.g.*, HF, MP2, B3LYP) were evaluated for deriving the ESP charges for the system. However, it was found that only M062X/6-311++g(3d,2p) derived charges could result in interaction parameters that were capable of predicting the phase diagram for the ternary system. This can be ascribed to the model's superiority in describing stacked interactions (π-π bonding) in the lutidine/*N*-oxide binary system since the other functionals (except MP2) cannot predict the parallel configuration of the pair (Zhao and Truhlar 2011). In this regard, some other functionals which belong to this family (*e.g.*, X3LYP, M06) also provide with the same values of partial charges for this system at 6-311++g(3d,2p) basis set.

Though the deviation between the experimental and simulation results were considerable, the CHELPG methodology gave an initial estimate of the partial charges. A second set of partial charges was selected to minimize the error between the experimental and theoretical phase separation curve. This was done by testing values in vicinity of the ESP charges in a heuristic manner. The partial charge set which provided the best result in terms of error has been included in the table. We can infer that for the *N*-oxide molecule, the final charges were almost similar to the ESP charges in both the dimers. On the other hand, the partial charge on '*O*' atom of water was overestimated by the population analysis. Similar deviations have been reported in literature (Martin and Zipse 2005). Finally, the partial charge on '*N*' atom of lutidine shows a positive deviation from the ESP charges for the lutidine/water system and a negative deviation for the lutidine/*N*-oxide system.

5.3. Conclusions

The three-component system of 2,6-lutidine/2,6-lutidine-*N*-oxide/water was studied using the UNIQUAC activity coefficient model and the ternary phase diagram was constructed at three different temperatures. The model parameters were derived from molecular simulations, which include the force field method and *ab initio* techniques. It was seen that the partial charges assigned to the atoms played an important role in the determination of the parameters while employing the force field. The partial charges determined by the CHELPG analysis provided an initial estimate for the interaction parameters. However the best values were obtained by following an empirical approach, wherein the objective was to reproduce the experimental data points for the ternary mixture. In future it would be worthwhile to examine the applicability of other force fields for calculating the interaction energies for the binary systems and compare the results with the current work.

6. CONCLUSIONS AND FUTURE WORK

This dissertation is aimed at improving the understanding of a complex reaction system and identifying possibilities for operating the reaction in an inherently safer manner. The reaction of interest was the *N*-oxidation of alkypyridines, which is mainly employed in the pharmaceutical industry. Many of hazards associated with the reaction are typical of other batch systems including the condition dependent decomposition of hydrogen peroxide and flammability of the reactants (alkylpyridines). The thermodynamics of the reaction mixture has a strong influence on the decomposition process especially in case of *N*-oxidation of higher order alkylpyridines where the alkylpyridine is immiscible in the aqueous phase. The current study provides experimental phase equilibrium data for the 2,6-lutidine *N*-oxidation system coupled with thermodynamic parameters obtained through computations. The results can be used to design inherently safer reactors that generate small amounts of waste chemicals during the production process. The research findings have been summarized in the subsection 6.1 while the future opportunities in this work have been outlined in subsection 6.2.

6.1. Conclusions

Experimental studies were conducted in the RC1*e* calorimeter to determine the effect of 2,6-lutidine-*N*-oxide on the 2,6-lutidine/water phase separation at 110 ^{o}C. Previous findings suggested that the immiscibility between the 2,6-lutidine and water, which is majorly responsible for accelerating the peroxide decomposition, is reduced by the 2,6-lutidine-*N*-oxide. The procedure employed in this work was based on dilution of two component (2,6-lutidine/2,6-

lutidine-*N*-oxide) and three component (2,6-lutidine/2,6-lutidine-*N*-oxide/water) mixtures with water. The mixtures were inspected visually and distinguished based on their appearance. Turbid appearance of the solution indicated that there was phase separation leading to formation of two phases. The ternary phase diagram for the mixture suggests that a single-phase solution will result if the *N*-oxide composition is above 20% (w/W).

It would be appropriate to envision this system as an oil/water/surfactant mixture wherein the *N*-oxide acts as a surfactant enhancing the interfacial interactions between the alkylpyridines and water. The *N*-oxide molecule consists of a hydrophillic end ($N^+ - O^-$) which aligns itself towards the water molecule leading to hydrogen bonding. Similarly, the benzene ring, which forms the hydrophobic end, shows affinity for the oil phase (alkylpyridine). Owing to this, the *N*-oxide molecule positions itself between the alkylpyridine and water and forms a self-assembled monolayer thereby reducing the interfacial energy and leading to homogenization. Several authors have observed this phenomenon with other liquid solutions containing oil-water mixtures (Jin, Parbhakar *et al.* 1997; Xu, Zhang *et al.* 2013; Nowak, Kovalchuk *et al.* 2016).

An attempt was made to extend the experimental work to other temperatures ($T = 115 - 125\ ^oC$) where the *N*-oxidation reaction is conducted. However, it was found that the phase separation compositions differed by a small amount within this temperature range. The current setup was unable to spot the difference accurately due to the error associated with measuring liquid compositions though it was possible to determine a general trend between the minimum *N*-oxide required for homogenization and temperature. Nevertheless, the phase equilibrium data can be used over the entire temperature range by including a safety factor while calculating the *N*-oxide

requirements for any semi-batch process. In addition to this, the study also provides information regarding the transition of two-phase systems into single-phase systems for the three-component mixture, which could be used to predict thermal runaways during the *N*-oxidation since the overall reaction rate depends on the mixing between the species. However, it is important to note that the effect of hydrogen peroxide and catalyst (phosphotungstic acid) has to be considered before adopting the current results.

The Fourier Transform Infrared (FTIR) spectroscopy was used to collect the absorption spectra of various binary and ternary mixtures of 2,6-lutidine, 2,6-lutidine-*N*-oxide and water. The characteristic peaks for individual species were tracked during the experiments. The data was used to identify solutions that have undergone phase separation to support the visual observations. In order to utilize the FTIR for measuring the component concentrations, it was necessary to calibrate the probe at the experimental conditions. Various ternary solutions were tested to construct the calibration model, which related the chemical compositions to the absorption peaks at the desired temperature. However, this model was ineffective in measuring the concentration of biphasic systems since they were based on data generated from single-phase mixtures. This was due the inability of the model to account for the synergistic effects between the compounds and lack of sensitivity of the probe.

The simulation work was conducted with an objective of exploring the possibility of utilizing computational chemistry for studying the present system. The major goal behind this study was to understand the molecular interactions in the mixture since it will have an effect on the overall *N*-oxidation reaction rate. Molecular dynamics simulations based on the Monte carlo technique

provided interaction energies for the various binary pairs which were used as parameters in the UNIQUAC activity coefficient model. When the theoretical results were compared with the experimental data it was found that the model predictions were fairly accurate. Apart from this, the methodology was used to examine the effect of temperature on the phase diagram.

It is important to note that a number of other simulation techniques were considered for determining the UNIQUAC parameters. For example, the molecular cluster method proposed by Sum and Sandler (1999) was followed and large molecular ensembles were constructed to estimate the binary interactions. However, the large size of the molecules present in the current system made it impossible to obtain a minimum energy configuration for the cluster because of many geometric degrees of freedom. The Monte Carlo sampling employed in the present research addressed this issue by testing several possible arrangements of the dimers.

The major contribution of this work was determining the thermodynamic parameters for the chemicals involved in the *N*-oxidation system, which will be useful in developing robust kinetic models for the reaction. Moreover, the binary parameters for the *N*-oxide based systems (2,6-lutidine-*N*-oxide/water and 2,6-lutidine-*N*-oxide/2,6-lutidine) were not available in open literature. These values can be used to study the VLE in *N*-oxide mixtures and determine the thermo-physical properties of *N*-oxide since the pure component properties for water and 2,6-lutidine are available.

6.2. Future Work

The *N*-oxidation of alkypyridines exhibits numerous challenges, which hamper of safety of the process. The following section provides recommendations for future work in this research area.

6.2.1. Calorimetric Studies

The *N*-oxidation of 2,6-lutidine should be performed with various starting mixtures of 2,6-lutidine-*N*-oxide and 2,6-lutidine and the system should be monitored continuously to check for phase separation (indicated by turbidity) during the reaction. Binary mixtures of 2,6-lutidine and 2,6-lutidine-*N*-oxide with the following compositions (90/10, 85/15, 80/20, 75/25, 60/40 wt.%) can be used for this purpose since these solutions were tested in this research. Also, the pressure rise during the reactions should be checked to determine the extent of peroxide decomposition during each of these cases. It is expected that the *N*-oxidation conducted with a 60/40 2,6-lutidine/2,6-lutidine-*N*-oxide mixture shows least amount of peroxide decomposition with a high product yield. It would be worthwhile to repeat the experiments for other temperatures between 110 ^{o}C and 125 ^{o}C. The peroxide dosing rate, stirring rate and catalyst quantities employed during the trials should be fixed based on the results obtained from 3-picoline *N*-oxidation (Pineda Solano 2014).

6.2.2. Thermodynamic Studies

The current study could be extended to include the effect of the catalyst (phosphotungstic acid) on the phase diagram. The catalyst is an ionic solid that dissociates in the liquid phase based on the chemical composition (Kozhevnikov 1987; Kozhevnikov, Sinnema *et al.* 1995; Kozhevnikov 2007). It is vital to understand this mechanism thoroughly before conducting experiments with the catalyst. Initial studies with *N*-oxide/water/catalyst mixtures suggest that the catalyst solubility reduces with the increase in water concentration at high temperatures (110 − 125 ^{o}C). This implies that *N*-oxide plays a pivotal role in dissolving the catalyst and maintaining complete homogeneity during *N*-oxidation. Information regarding the catalyst solubility in the reaction mixture will assist the process of downstream separation. Once this data is available, the Gibbs minimization method can be used to combine the chemical equilibrium with the phase equilibrium to study both the situations simultaneously.

The present work could also be extended to other higher order alkylpyridines (for *e.g.*, 2,4,6-collidine) to verify if a similar relation exists between the aqueous solutions of the alkylpyridine and their corresponding *N*-oxides.

REFERENCES

Abrams, D. S. and J. M. Prausnitz (1975). "Statistical thermodynamics of liquid mixtures: a new expression for the excess Gibbs energy of partly or completely miscible systems." AIChE journal **21**(1): 116-128.

Adcock, S. A. and J. A. McCammon (2006). "Molecular Dynamics: Survey of Methods for Simulating the Activity of Proteins." Chemical Reviews **106**(5): 1589-1615.

Al−Alawi, A., F. R. van de Voort and J. Sedman (2005). "A new FTIR method for the analysis of low levels of FFA in refined edible oils." Spectroscopy letters **38**(4-5): 389-403.

Allen, M. P. (2004). "Introduction to molecular dynamics simulation." Computational soft matter: from synthetic polymers to proteins **23**: 1-28.

Andon, R. and J. Cox (1952). "896. Phase relationships in the pyridine series. Part I. The miscibility of some pyridine homologues with water." Journal of the Chemical Society: 4601-4606.

Aspen Plus Version 8.2, A. T. I. "Cammbridge, MA, USA."

Becke, A. D. (1993). "Density−functional thermochemistry. III. The role of exact exchange." The Journal of Chemical Physics **98**(7): 5648-5652.

Beveridge, D. L. and F. DiCapua (1989). "Free energy via molecular simulation: applications to chemical and biomolecular systems." Annual review of biophysics and biophysical chemistry **18**(1): 431-492.

Blanco, M. (1991). "Molecular silverware. I. General solutions to excluded volume constrained problems." Journal of Computational Chemistry **12**(2): 237-247.

Bondi, A. (1964). "van der Waals Volumes and Radii." Journal of physical chemistry **68**(3): 441-451.

Breneman, C. M. and K. B. Wiberg (1990). "Determining atom−centered monopoles from molecular electrostatic potentials. The need for high sampling density in formamide conformational analysis." Journal of Computational Chemistry **11**(3): 361-373.

Brubach, J. B., A. Mermet, A. Filabozzi *et al.* (2005). "Signatures of the hydrogen bonding in the infrared bands of water." The Journal of Chemical Physics **122**(18): 184509.

Campos-Martin, J. M., G. Blanco-Brieva and J. L. G. Fierro (2006). "Hydrogen Peroxide Synthesis: An Outlook beyond the Anthraquinone Process." Angewandte Chemie International Edition **45**(42): 6962-6984.

Cha, T.-H. and J. M. Prausnitz (1985). "Thermodynamic method for simultaneous representation of ternary vapor-liquid and liquid-liquid equilibria." Industrial & Engineering Chemistry Process Design and Development **24**(3): 551-555.

Chen, J. R. (2004). "An inherently safer process of cyclohexane oxidation using pure oxygen—an example of how better process safety leads to better productivity." Process Safety Progress **23**(1): 72-81.

Coates, J. (2000). "Interpretation of infrared spectra, a practical approach." Encyclopedia of analytical chemistry.

Conner, W. (1993). Hydrogen peroxide safety issues, EG and G Rocky Flats, Inc., Golden, CO (United States). Rocky Flats Plant. Funding organisation: USDOE, Washington, DC (United States).

Connolly, M. L. (1983). "Analytical molecular surface calculation." Journal of Applied Crystallography **16**(5): 548-558.

Cox, J. and E. Herington (1956). "The coexistence curve in liquid-liquid binary systems." Trans. Faraday Soc. **52**: 926-930.

Das, A., P. Sahu and S. M. Ali (2017). "Molecular Dynamics Simulation for the Calibration of the OPLS Force Field Using DFT Derived Partial Charges for the Screening of Alkyl Phosphate Ligands by Studying Structure, Dynamics, and Thermodynamics." Journal of Chemical & Engineering Data **62**(8): 2280-2295.

Dove, M. T. (2008). "An introduction to atomistic simulation methods." Seminarios de la SEM **4**: 7-37.

Edwards, V. H. (2011). "Designing safer process plants." Chemical Engineering Progress **118**(4): 44-48.

Fan, C. U. N. F. (1992). "Application of molecular simulation to derive phase diagrams of binary mixtures." Macromolecules **25**(14): 3667.

Flemr, V. (1976). "A note on excess Gibbs energy equations based on local composition concept." Collection of Czechoslovak Chemical Communications **41**(11): 3347-3349.

Frisch, M. J., G. W. Trucks, H. B. Schlegel *et al.* (2009). Gaussian 09, Revision B.01. Wallingford CT.

Fujiwara, M., P. S. Chow, D. L. Ma *et al.* (2002). "Paracetamol Crystallization Using Laser Backscattering and ATR-FTIR Spectroscopy: Metastability, Agglomeration, and Control." Crystal Growth & Design **2**(5): 363-370.

Gao, J. and M. Papadaki (2006). "Global kinetic model: A case study on the N-oxidation of alkylpyridines." Journal of Hazardous Materials **130**(1): 141-147.

Grattoni, C. A., R. A. Dawe, C. Y. Seah *et al.* (1993). "Lower critical solution coexistence curve and physical properties (density, viscosity, surface tension, and interfacial tension) of 2, 6-lutidine+ water." Journal of Chemical and Engineering Data **38**(4): 516-519.

Green, J., D. Harrison, W. Kynaston *et al.* (1970). "The vibrational spectra of the dimethylpyridines." Spectrochimica Acta Part A: Molecular Spectroscopy **26**(11): 2139-2146.

Greene, B., D. L. Baker and W. Frazier (2005). "Hydrogen peroxide accidents and incidents: What we can learn from history, NASA In-house document. WSTF-RD-0972-001-03."

Guggenheim, E. A. (1952). Mixtures: the theory of the equilibrium properties of some simple classes of mixtures, solutions and alloys, Clarendon Press.

Janardanan, S., M. I. Papadaki, S. P. Waldram *et al.* (2017). "Toward an inherently safer alternative for operating N-oxidation of alkylpyridines: Effect of N-oxide on lutidine – water phase separation." Thermochimica acta **656**(Supplement C): 38-46.

Janardanan, S., L. M. Perez and M. S. Mannan (2018). "Study of phase behavior of 2, 6-lutidine, 2, 6-lutidine-N-oxide and water mixture using UNIQUAC model with interaction parameters determined by molecular simulations." Thermochimica acta.

Jin, J.-M., K. Parbhakar and L. Dao (1997). "Model for water-in-oil microemulsions: surfactant effects." Physical Review E **55**(1): 721.

Jones, C. W. (1999). Applications of Hydrogen Peroxide and Derivatives, Royal Society of Chemistry.

Jones, C. W. (1999). Applications of hydrogen peroxide and derivatives., Cambridge, UK : Royal Society of Chemistry.

Jónsd, S. Ó., K. Rasmussen and A. Fredenslund (1994). "UNIQUAC parameters determined by molecular mechanics." Fluid Phase Equilibria **100**: 121-138.

Jónsdóttir, S. Ó., R. A. Klein and K. Rasmussen (1996). "UNIQUAC interaction parameters for alkane/amine systems determined by Molecular Mechanics." Fluid Phase Equilibria **115**(1-2): 59-72.

Jorgensen, W. L. and N. A. McDonald (1998). "Development of an all-atom force field for heterocycles. Properties of liquid pyridine and diazenes." Journal of Molecular Structure: THEOCHEM **424**(1): 145-155.

Kamath, G., N. Lubna and J. J. Potoff (2005). "Effect of partial charge parametrization on the fluid phase behavior of hydrogen sulfide." The Journal of Chemical Physics **123**(12): 124505.

Karplus, M. and G. A. Petsko (1990). "Molecular dynamics simulations in biology." Nature **347**(6294): 631.

Ketko, M. B. H. and J. J. Potoff (2007). "Effect of partial charge parameterization on the phase equilibria of dimethyl ether." Molecular Simulation **33**(9-10): 769-776.

Kletz, T. (1978). "What you don't have, can't leak." Chemistry and Industry **6**: 287-292.

Kletz, T. (1985). "Inherently safer plants." Plant/Operations Progress **4**(3): 164-167.

Kozhevnikov, I. (1987). "Advances in catalysis by heteropolyacids." Russian Chemical Reviews **56**(9): 811.

Kozhevnikov, I. (2007). "Sustainable heterogeneous acid catalysis by heteropoly acids." Journal of Molecular Catalysis A: Chemical **262**(1): 86-92.

Kozhevnikov, I., A. Sinnema and H. Van Bekkum (1995). "Proton sites in Keggin heteropoly acids from17O NMR." Catalysis letters **34**(1-2): 213-221.

Kumasaki, M. (2006). "An explosion of a tank car carrying waste hydrogen peroxide." Journal of Loss Prevention in the Process Industries **19**(4): 307-311.

Lee, C., W. Yang and R. G. Parr (1988). "Development of the Colle-Salvetti correlation-energy formula into a functional of the electron density." Physical review B **37**(2): 785.

Lewiner, F., G. Févotte, J. P. Klein *et al.* (2001). "Improving batch cooling seeded crystallization of an organic weed-killer using on-line ATR FTIR measurement of supersaturation." Journal of Crystal Growth **226**(2–3): 348-362.

Lewiner, F., J. P. Klein, F. Puel *et al.* (2001). "On-line ATR FTIR measurement of supersaturation during solution crystallization processes. Calibration and applications on three solute/solvent systems." Chemical Engineering Science **56**(6): 2069-2084.

Lin, S. T. and S. I. Sandler (1999). "Infinite dilution activity coefficients from ab initio solvation calculations." AIChE Journal **45**(12): 2606-2618.

Malaspina, T., K. Coutinho and S. Canuto (2002). "Ab initio calculation of hydrogen bonds in liquids: A sequential Monte Carlo quantum mechanics study of pyridine in water." The Journal of Chemical Physics **117**(4): 1692-1699.

Martin, F. and H. Zipse (2005). "Charge distribution in the water molecule—A comparison of methods." Journal of Computational Chemistry **26**(1): 97-105.

McDermott, C. and N. Ashton (1977). "Note on the definition of local composition." Fluid Phase Equilibria **1**(1): 33-35.

Mettler-Toledo (2012). "Hardware Manual: ReactIR 15^{TM} - Improving Chemistry Understanding."

Mettler-Toledo (2012). "RC1*e* High Performance Thermostat - Operating Instructions."

Miertuš, S., E. Scrocco and J. Tomasi (1981). "Electrostatic interaction of a solute with a continuum. A direct utilizaion of AB initio molecular potentials for the prevision of solvent effects." Chemical Physics **55**(1): 117-129.

Misono, M., I. Ono, G. Koyano *et al.* (2000). "Heteropolyacids. Versatile green catalysts usable in a variety of reaction media." Pure and applied chemistry **72**(7): 1305-1311.

Nagata, I. and Y. Usui (1989). "Correlation of ternary liquid-liquid equilibrium data and prediction of quaternary liquid-liquid equilibrium data by means of the uniquac model." Thermochimica acta **140**: 121-138.

Nowak, E., N. M. Kovalchuk, Z. Che *et al.* (2016). "Effect of surfactant concentration and viscosity of outer phase during the coalescence of a surfactant-laden drop with a surfactant-free drop." Colloids and Surfaces A: Physicochemical and Engineering Aspects **505**: 124-131.

Oh, S. Y. and Y. C. Bae (2010). "Phase Equilibrium Calculations of Ternary Liquid Mixtures with Binary Interaction Parameters and Molecular Size Parameters Determined from Molecular Dynamics." The Journal of Physical Chemistry B **114**(27): 8948-8953.

Oliveira, J. S., R. Montalvão, L. Daher *et al.* (2006). "Determination of methyl ester contents in biodiesel blends by FTIR-ATR and FTNIR spectroscopies." Talanta **69**(5): 1278-1284.

Painter, P. C., M. M. Coleman, R. G. Jenkins *et al.* (1978). "Fourier transform infrared study of mineral matter in coal. A novel method for quantitative mineralogical analysis." Fuel **57**(6): 337-344.

Palomo-Coll, A. (1992). "A process for the preparation of omeprazol, ES 2026761 (A6)." European Patent Office.

Papadaki, M., R. J. Emery, E. Serra *et al.* (2002). "Sensitivity analysis of the 2-methylpyridine N-oxidation kinetic model." Green Chemistry **4**(3): 199-205.

Papadaki, M. and J. Gao (2005). "Kinetic models of complex reaction systems." Computers & chemical engineering **29**(11): 2449-2460.

Papadaki, M. and J. Gao (2005). "Kinetic models of complex reaction systems." Computers & chemical engineering **29**(11-12): 2449-2460.

Papadaki, M., E. Marqués-Domingo, J. Gao *et al.* (2005). "Catalytic decomposition of hydrogen peroxide in the presence of alkylpyridines: Runaway scenarios studies." Journal of Loss Prevention in the Process Industries **18**(4): 384-391.

Papadaki, M. and H. P. Nawada (2003). "Towards improved reaction runaway assessment methods I. Simple calorimetric method of evaluation of heat transfer coefficient and reactor thermal mass." International Journal of Chemical Reactor Engineering **1**(1): 40.

Papadaki, M., V. Stoikou, D. Mantzavinos *et al.* (2002). "Towards improved reaction runaway studies: kinetics of the N-oxidation of 2-methylpyridine using heat-flow calorimetry." Process Safety and Environmental Protection **80**(4): 186-196.

Pascual−Ahuir, J., E. Silla, J. Tomasi *et al.* (1987). "Electrostatic interaction of a solute with a continuum. Improved description of the cavity and of the surface cavity bound charge distribution." Journal of Computational Chemistry **8**(6): 778-787.

Pascual−ahuir, J.-L., E. Silla and I. Tunon (1994). "GEPOL: An improved description of molecular surfaces. III. A new algorithm for the computation of a solvent−excluding surface." Journal of Computational Chemistry **15**(10): 1127-1138.

Pascual−Ahuir, J. L. and E. Silla (1990). "GEPOL: An improved description of molecular surfaces. I. Building the spherical surface set." Journal of Computational Chemistry **11**(9): 1047-1060.

Pineda Solano, A. L. (2014). Design of Inherently Safer Complex Reactive Processes: Application on the N-Oxidation of Alkylpyridines.

Pineda-Solano, A. (2014). Design of Inherently Safer Complex Reactive Processes: Application on the N-Oxidation of Alkylpyridines, Texas A&M University.

Pineda-Solano, A., L. Saenz-Noval, S. Nayak *et al.* (2012). "Inherently safer reactors: Improved efficiency of 3-picoline N-oxidation in the temperature range 110–125°C." Process Safety and Environmental Protection **90**(5): 404-410.

Prausnitz, J. M. (1980). Computer calculations for multicomponent vapor-liquid and liquid-liquid equilibria, Prentice Hall.

Ren, H., Q. Zhang, X. Chen *et al.* (2007). "A molecular simulation study of a series of cyclohexanone formaldehyde resins: Properties and applications in plastic printing." Polymer **48**(3): 887-893.

Richards, F. M. (1977). "Areas, volumes, packing, and protein structure." Annual review of biophysics and bioengineering **6**(1): 151-176.

Saenz, L., V. C. Vazquez, L. Liu *et al.* (2009). "2-Methylpyridine-N-oxidation runaway studies." Journal of Loss Prevention in the Process Industries **22**(6): 839-843.

Saenz, L. R., V. H. Carreto-Vazquez, W. J. Rogers *et al.* (2011). "Thermal decomposition of 2-methylpyridine N-oxide: Effect of temperature and influence of phosphotungstic acid as the catalyst." Catalysis Communications **12**(14): 1370-1373.

Saenz-Noval, L. R. (2011). Evaluation of alternatives for safer and more efficient reactions: a study of the N-oxidation of alkylpyridines, Texas A&M University.

Sahandzhieva, K., D. Tuma, S. Breyer *et al.* (2006). "Liquid− liquid equilibrium in mixtures of the ionic liquid 1-n-butyl-3-methylimidazolium hexafluorophosphate and an alkanol." Journal of Chemical & Engineering Data **51**(5): 1516-1525.

Scriven, E. F. V. and R. Murugan (2000). Pyridine and Pyridine Derivatives. Kirk-Othmer Encyclopedia of Chemical Technology, John Wiley & Sons, Inc.

Sempere, J., R. Nomen, J. Rodriguez *et al.* (1998). "Modelling of the reaction of N-oxidation of 2-methylpyridine using hydrogen peroxide and a complex metal catalyst." Chemical Engineering and Processing: Process Intensification **37**(1): 33-46.

Shimizu, S., N. Watanabe, T. Kataoka *et al.* (1993). "Pyridine and pyridine derivatives." Ullmann's Encyclopedia of Industrial Chemistry.

Shimizu, S., N. Watanabe, T. Kataoka *et al.* (2000). "Pyridine and pyridine derivatives." Ullmann's Encyclopedia of Industrial Chemistry.

Silla, E., I. Tunon and J. L. Pascual−Ahuir (1991). "GEPOL: An improved description of molecular surfaces II. Computing the molecular area and volume." Journal of Computational Chemistry **12**(9): 1077-1088.

Silla, E., F. Villar, O. Nilsson *et al.* (1990). "Molecular volumes and surfaces of biomacromolecules via GEPOL: A fast and efficient algorithm." Journal of molecular graphics **8**(3): 168-172.

Sørensen, J. M., T. Magnussen, P. Rasmussen *et al.* (1979). "Liquid—liquid equilibrium data: Their retrieval, correlation and prediction Part II: Correlation." Fluid Phase Equilibria **3**(1): 47-82.

Stephenson, R. M. (1993). "Mutual solubility of water and pyridine derivatives." Journal of Chemical and Engineering Data **38**(3): 428-431.

Sum, A. K. and S. I. Sandler (1999). "A Novel Approach to Phase Equilibria Predictions Using Ab Initio Methods." Industrial & Engineering Chemistry Research **38**(7): 2849-2855.

Sum, A. K. and S. I. Sandler (1999). "Use of ab initio methods to make phase equilibria predictions using activity coefficient models." Fluid Phase Equilibria **158**: 375-380.

Sun, H. (1998). "COMPASS: An ab Initio Force-Field Optimized for Condensed-Phase ApplicationsOverview with Details on Alkane and Benzene Compounds." The Journal of Physical Chemistry B **102**(38): 7338-7364.

Swann, G. E. and S. Patwardhan (2011). "Application of Fourier Transform Infrared Spectroscopy (FTIR) for assessing biogenic silica sample purity in geochemical analyses and palaeoenvironmental research." Climate of the Past **7**(1): 65-74.

Swinehart, D. F. (1962). "The Beer-Lambert Law." Journal of Chemical Education **39**(7): 333.

Treybal, R. E. (1963). Liquid extraction, McGraw-Hill.

ULBERTH, F. and H. J. HAIDER (1992). "Determination of low level trans unsaturation in fats by Fourier transform infrared spectroscopy." Journal of food science **57**(6): 1444-1447.

United States Chemical Safety and Hazard Investigation Board (2002). "Hazard Investigation: Improving Reactive Hazard Management, CSB Report No. 2001-01-H."

van de Voort, F. R., A. A. Ismail, J. Sedman *et al.* (1994). "The determination of peroxide value by fourier transform infrared spectroscopy." Journal of the American Oil Chemists' Society **71**(9): 921-926.

van Gunsteren, W. F. and H. J. Berendsen (1990). "Computer simulation of molecular dynamics: Methodology, applications, and perspectives in chemistry." Angewandte Chemie International Edition **29**(9): 992-1023.

Wei, C., W. J. Rogers and M. S. Mannan (2004). "Application of screening tools in the prevention of reactive chemical incidents." Journal of Loss Prevention in the Process Industries **17**(4): 261-269.

Wilson, G. M. (1964). "Vapor-Liquid Equilibrium. XI. A New Expression for the Excess Free Energy of Mixing." Journal of the American Chemical Society **86**(2): 127-130.

Xu, J., Y. Zhang, H. Chen *et al.* (2013). "Effect of surfactant headgroups on the oil/water interface: An interfacial tension measurement and simulation study." Journal of Molecular Structure **1052**: 50-56.

Yang, J. H. and Y. C. Bae (2008). "Phase behaviors of polymer solutions using molecular simulation technique." The Journal of Chemical Physics **129**(6): 064902.

Yaws, C. L. (2012). Yaws' critical property data for chemical engineers and chemists. Norwich, N.Y., Knovel.

Zhao, Y. and D. G. Truhlar (2008). "The M06 suite of density functionals for main group thermochemistry, thermochemical kinetics, noncovalent interactions, excited states, and

transition elements: two new functionals and systematic testing of four M06-class functionals and 12 other functionals." Theoretical Chemistry Accounts **120**(1): 215-241.

Zhao, Y. and D. G. Truhlar (2011). "Applications and validations of the Minnesota density functionals." Chemical Physics Letters **502**(1): 1-13.